

ABSTRACT

Title of Thesis: CATALYTIC BEHAVIOR OF METAL-ORGANIC FRAMEWORK UiO-66 IN CONVERSION OF SACCHARIDE BIOMASS

Ricardo D. Morales, Master's of Science, 2018

Directed By: Professor, Dr. Dongxia Liu, Department of Chemical and Biomolecular Engineering

UiO-66 (Universitet i Oslo 66) is a zirconium-based metal-organic framework (MOF) material. Due to the superior thermal, chemical and mechanical stability, UiO-66 is one of the most attractive MOF platforms to enabling catalysis. This thesis explored the catalytic behavior of UiO-66 in saccharide biomass conversion. The Brønsted acidity in UiO-66 enabled depolymerization of inulin into monosaccharides, which has distinct high activity than inorganic BEA zeolite and aqueous hydrogen chloride (HCl) acid catalysts. The catalytic mechanism of UiO-66 stays in-between pore mouth catalysis and random chain splitting which are prevalent mechanisms in BEA and HCl acid, respectively. The UiO-66 was further explored as catalyst for synthesis of alkyl lactates from saccharide biomass via one-pot multiple step reaction approach. The Lewis and Brønsted acidity in UiO-66 enabled this reaction network, and produced methyl and ethyl lactate from methanol and ethanol solvents by using mono-, di- and polysaccharide feedstocks.

CATALYTIC BEHAVIOR OF METAL-ORGANIC FRAMEWORK UIO-66 IN
CONVERSION OF SACCHARIDE BIOMASS

By

Ricardo Daniel Morales

Thesis submitted to the Faculty of the Graduate School of the
University of Maryland, College Park, in partial fulfillment
of the requirements for the degree of
Master of Science
2018

Advisory Committee:
Professor Dongxia Liu, Chair
Professor Peter Kofinas
Professor Kyu Yong Choi

© Copyright by
Ricardo Daniel Morales
2018

Dedication

This work is dedicated to my parents, Ricardo M. and Margarita R. Morales, who have always advocated the power of higher education, and to the rest of my friends, family, and colleagues for their support at every step of the way.

Acknowledgements

I would like to acknowledge the mentorship of my advisor, Dr. Dongxia Liu, for her guidance and leadership throughout my research since I was an undergraduate with no research experience. Throughout the years, she has helped to instill in me an appreciation and passion for the research process.

I would also like to thank my fellow lab mates for always being there to help me with lab equipment, instrumentation, analysis and teaching me so much in general. Lastly, I would like to acknowledge my professors here at Maryland, who have helped me learn and appreciate the field of chemical engineering, especially Dr. Peter Kofinas and Professor Kyu Yong Choi for agreeing to serve on my committee.

Table of Contents

Dedication	ii
Acknowledgements	iii
Table of Contents	iv
List of Tables and Schemes	v
List of Figures	vi
Chapter 1: Introduction.....	1
Chapter 2: UiO-66 Synthesis and Characterization	10
Chapter 3: Inulin Hydrolysis on Brønsted Acid Sites in UiO-66: A Catalytic Behavior In-Between Random Chain Scission and Pore Mouth Catalysis.....	18
Chapter 4: Saccharide Conversion to Lactic Acid Derivatives with Lewis and Brønsted acidic UiO-66 catalyst	52
Chapter 5: Conclusions and Future Work.....	66
References:.....	68

List of Tables and Schemes

Table 2-1. Textural property of UiO-66 catalysts.....	14
Table 3-1. Textural property and acidity of BEA and UiO-66 catalysts.....	26
Table 3-2. Kinetic model fit parameters for Kuhn's and Exo-Enzymatic Models with R^2 values for each fit.....	50
Scheme 3-1. Inulin hydrolysis to different saccharide products.....	19
Scheme 3-2. Proposed Kuhn's reaction mechanism for inulin hydrolysis via indiscriminant statistical splitting.....	38
Scheme 3-3. Proposed exo-enzymatic reaction mechanism for inulin hydrolysis via pore-mouth catalysis.....	42

List of Figures

Figure 2-1. Crystalline structure of UiO-66 as well as characteristic metal oxide clusters and BDC organic linkers. ⁵⁵	10
Figure 2-2. Characterization results for UiO-66 catalyst using A) wide angle XRD measurement, B) N ₂ adsorption-desorption isotherms for UiO-66, C) FTIR spectroscopy for UiO-66 and BDC, and D) thermogravimetric analysis.	14
Figure 2-3. TGA graphical representation for ligand defect calculation.	16
Figure 3-1. A) Pore size distributions, and B) N ₂ adsorption-desorption isotherms for UiO-66 and BEA.	24
Figure 3-2. HPLC-RID chromatogram of saccharide peaks.	27
Figure 3-3. Percent conversion for inulin hydrolysis versus reaction time over A) UiO-66, B) BEA, C) HCl acid (pH of 1.57), and D)BDC acid respectively.	29
Figure 3-4. Product selectivity and conversion comparison for different catalyst conditions of A) BEA, B) UiO-66, C) HCl acid conditions for all temperature conditions.	32
Figure 3-5. Product formation concentrations for Glucose and Fructose (A) and Sucrose and Fructose (B) for catalyst conditions of UiO-66, BEA, and HCl acid (pH 1.5-2.0).....	35
Figure 3-6. Monomer concentration versus reaction time, with Kuhn’s kinetic model fitting for (A) UiO-66, (B) BEA, and (C) HCl (pH of 1.57) at different temperatures.....	39
Figure 3-7. Monomer concentration versus reaction time, with Exo-Enzymatic kinetic model fitting for (A) UiO-66, (B) BEA, and (C) HCl (pH of 1.57) at different temperatures.	45
Figure 3-8. Monomer concentration over time, with Kuhn’s and Exo-Enzymatic kinetic model fitting for (A) UiO-66 at 341K, (B) BEA at 363 K, and (C) HCl at 353 K(pH of 1.57)	46
Figure 4-1. Monosugar Conversion Results for UiO-66 and no catalyst present denoted as “Blank” for fructose in methanol and ethanol (A and B) respectively; and glucose in methanol and ethanol (C and D) respectively.....	58
Figure 4-2. Product yield for fructose as a reactant with UiO-66 catalyst condition in (A) methanol and (B) ethanol.....	60
Figure 4-3. Product yield for glucose as a reactant with UiO-66 catalyst condition in (A) methanol and (B) ethanol.....	61
Figure 4-4. Sucrose Conversion Results for UiO-66 and no catalyst present denoted as “Blank” for fructose in methanol and ethanol (A and B) respectively.	62
Figure 4-5. Product yield for sucrose as a reactant with UiO-66 catalyst condition in (A) methanol and (B) ethanol.....	62
Figure 4-6. Product yields for inulin as a reactant with UiO-66 catalyst condition in (A) methanol and (B) ethanol.....	64

Chapter 1: Introduction

1.1. Background on nanoporous materials

Nanoporous materials are comprised of either an organic or inorganic framework with a porous morphology defined by pore diameters of 100 nm or smaller. Conventionally, pore sizes are used to further classify nanoporous materials: microporous materials (pore size 0.2-2 nm); mesoporous materials (pore size 2 nm-50 nm); and macroporous materials (pore size 50-1000 nm) ^{1, 2}. Defining characteristics of nanoporous materials are high surface areas and pore volumes. Materials with these characteristics are ideally suited for a variety of applications such as adsorption, gas separation, and heterogeneous catalysis. Heterogeneous catalysis is vital to the chemical industry as the majority of industrial catalysts are high-surface area solids with active moieties well dispersed throughout. ³ Zeolites have traditionally been the industry standard for heterogeneous catalysis. However, within the past two decades, metal organic frameworks have arisen as a new, promising alternative to the more traditional zeolites already extensively studied.

1.2. Zeolite materials

Zeolites are aluminosilicate porous crystalline minerals first discovered in 1756 by Axel Fredrik Cronstedt. He observed that a mineral, stillbite, lost a significant amount of water when heated, hence the word “zeolite” (“zeo” meaning “to boil” and “lithos” meaning “stone.”) ⁴ Since then, over 40 natural zeolite frameworks have been discovered and more than 200 synthetic zeolites have been created. ⁵ With the advent of the petroleum industry, synthetic zeolites became the dominant platform solid acid catalyst used in fluid catalytic cracking (FCC) units. ⁶

Zeolites are composed of SiO_4 tetrahedral-coordinated units with AlO_4^- ions substituted throughout its framework. These two individual tetrahedrons serve as the primary building units. Secondary building units are comprised of four or more primary units put together. The three dimensional structure of zeolites is determined by the arrangement of secondary building units. ⁷

An analogous example of how these building units assemble would be an enzyme. The primary building units of an enzyme would be the individual amino acids, and the secondary building unit would be the protein sequence of amino acids chained together. The 3D structure of the enzyme would result from the secondary building unit sequence folding together. Like proteins, the different arrangements of these secondary building units can lead to over a million different possible zeolite structures.

1.2.1 Synthesis of zeolites

Although some zeolites are naturally occurring mineral formations, synthetic zeolites are typically produced through hydrothermal synthesis ⁸. Amorphous silica and alumina precursors are mixed at specific ratios and form crystalline structures with the use of structure directing agents, mineralizing agents, and supersaturated alkaline solution. ⁹

Mineralizing agents allow the precursors to move freely in the gel solution, and ¹⁰ supersaturated aqueous alkaline solution promotes the mixing of the various gel components and plays a key role in the crystallization process. After the gel is mixed for some time under constant temperature (the aging process), it is crystallized under hydrothermal conditions. The last step removes any left-over structure directing agents by heating the zeolite at 773-873 K, isolating the zeolite. ¹¹

Zeolites are metastable species which will form more dense structures over time; as a result, each structure is very sensitive to variations in synthesis conditions (i.e. pH, aging time, etc.), so changes in any of these parameters can result in different crystal sizes, crystal types, and even different zeolites themselves.¹²

1.3. Metal organic framework materials

Metal organic frameworks (MOFs) are nanoporous materials that have garnered a lot of attention in recent years. Metal organic frameworks are composed of metal oxide units connected by organic linkers. Compared to zeolites, metal organic framework development is still relatively young, with their development starting in the 1990s as coordination chemists began to investigate the assembly of organic and inorganic building blocks for porous structures.¹³ One of the initial challenges in developing MOFs was achieving thermal and chemical stability, but since then, several stable MOFs have emerged.¹⁴

1.3.1 Metal organic framework structure

The metal oxides in MOFs are the structural building units (SBUs) which are connected by organic linkers. Different metal oxide SBUs will have different coordination numbers, therefore, the type of SBU will determine where the organic linkers attach to the SBU; this is crucial in determining the ultimate crystalline structure of the MOF.¹⁵

SBUs by themselves are very important to the crystalline structure of MOFs, however, the introduction of organic ligands can result in even more diversity among MOFs. A common attribute found in organic linkers is a carboxylic acid group on both ends of these symmetrical organic molecules. Examples of organic ligands include oxalic

acid, malonic acid, succinic acid, and terephthalic acid (BDC). These COOH groups bond to the SBU coordination complexes in order to form the structural matrix. The smaller the organic linkers, the shorter the distance between the SBUs, leading the organic linkers to be pivotal to the structure's intrinsic porosity when guest molecules such as DMF solvent are removed.¹⁶

1.3.2 Functionalization of MOFs

One of the advantages unique to MOFs is the ease of customizing the catalyst properties with the use of functionalized groups (-SO₃, -NH₂, -COOH, etc.) These groups can be intrinsically embedded in the crystalline framework by being introduced through the organic ligands.¹⁷ Further tuning of functionalized groups can be achieved by combining functionalized organic ligands at different molar ratios to the same non-functionalized organic ligand.¹⁸

1.3.3 Synthesis of MOFs

The main strategy in the synthesis of MOFs is to create defined inorganic SBUs without the loss of the organic linker while simultaneously allowing nucleation and crystal growth to occur.¹⁹ Solvothermal and non-solvothermal methods involve synthesis temperatures held above or below solvent boiling points respectively. Changes in solvothermal conditions like pressure, time or concentration can produce different materials.²⁰ Solvothermal synthesis methods provide advantages to conventional methods because they can produce compounds containing elements in oxidation states that would otherwise be difficult to obtain.²¹ Solvothermal synthesis performed in aqueous media is

referred to as hydrothermal synthesis. The reagents in zeolite synthesis are typically soluble in water, so hydrothermal synthesis is preferred for zeolites.

However, for metal organic frameworks, the organic ligands are seldom soluble in water, so solvothermal synthesis in organic solvents is preferred. A notable exception Fe-MIL-100, which is synthesized in hydrothermal conditions.²² To grow crystals from clear solutions, it is necessary to exceed the critical nucleation concentration. This is conventionally achieved through solvent evaporation, which is why solvothermal synthesis requires temperatures above the boiling points of the solvents.^{19, 23} Stainless steel autoclaves are therefore typically required, as they can withstand high temperature and pressure conditions. After the crystal collection, usually performed using filtration or centrifugation, excess organic ligand is removed through washing.

In addition to solvothermal synthesis, another conventional method of MOF synthesis is non-solvothermal synthesis. This occurs in a non-aqueous solvent but uses temperature conditions below the boiling point of the solvent. Popular MOFs including MOF-5, MOF-74, MOF-177, HKUST-1, and ZIF-8, can be synthesized at by mixing the reagents at room temperature.²⁴ Under this direct precipitation method, the crystallization takes place very rapidly relative to the kinetics of solvothermal processes. These processes tend to yield smaller crystals compared to crystals produced via solvothermal synthesis.

As MOFs become increasingly popular, novel synthesis methods have been explored to produce MOFs at larger scales. One off the most prominent methods is microwave-assisted synthesis. This well-established process originating from synthetic chemistry has been proven to accelerate organic metallic synthesis methods since the early 1990s.²⁵ Microwaves use electromagnetic radiation to heat the entirety of a solution,

resulting in a heating process is not only energy efficient but also facilitates rapid nucleation. Overall, microwave heating can produce high yields of desirable product. Some drawbacks to microwave heating are related to the instrumentation which varies between microwaves, introducing a challenge when attempting to reproduce irradiation power and, as a result, time of reaction and temperature.²⁶ MOFs produced via this method are generally metal(II) and metal(III) carboxylate-based MOFs such as Cr-MIL-100 and HKUST-1.^{27, 28}

Electrochemical synthesis is a method first created by BASF in 2005. This process works by continuously adding metal ions to reaction medium with anionic dissolution of organic ligand and protic solvent (to avoid metal deposition on the cathode).²⁹ Primarily Cu- and Zn- MOFs have combined with bulky aromatic ligands such as 1,4 benzodicarboxylic acid (BDC) and biphenyl-4,4'-dicarboxylate (BPDC) or imidazolate organic ligands. The most studied MOF from this method has been HKUST-1. Electrochemical synthesis allows for metal-salt free and continuous production of MOF.³⁰

Mechanochemical synthesis is another alternative method for MOF crystal growth. The idea is to induce mechanical breakage of intramolecular bonds and subsequently chemically transform the material into the desired state. This form of crystal growth is well established in pharmaceuticals, organic synthesis, and polymer synthesis.³¹ Since 2006, mechanochemical synthesis has been applied to MOF development with one potential application being for solvent-free MOF synthesis.³²

Sonochemical synthesis uses high frequency, cyclic mechanical vibrations to create small, alternating, compressive pressure regions in a solution. These alternating pressure regions form small, unstable micro-bubbles, which very quickly burst. The process of

constant formation and bursting of these small bubbles, known as cavitation, which leads to local hotspots of high temperature and pressure at short time scales.² The high shear forces produced from the constantly-bursting micro-bubbles produce similar effects to mechanochemical synthesis. The most extensively studied MOF developed using this process has been HKUST-1. Starting from copper acetate and H₃BDC, small HKUST-1 (10-40 nm) crystals were formed after 5 minutes at room temperature.³³ The advantage of low temperature and fast crystallization kinetics make sonochemical synthesis a promising route for fabricating MOFs.

1.3.4 Applications of MOFs

MOFs can support permanent porosity and exhibit exclusion properties that traditional zeolites and other inorganic porous materials do not display when used for gas sorption.³⁴ One advantage that MOFs have over zeolites for gas storage is that, because they are largely organic, they are lighter than aluminosilicate zeolites, which have an entirely-metal framework. Zeolites therefore have an inherent disadvantage for meeting ambitious Department of Energy targets for hydrogen storage compared to lighter MOFs and carbon frameworks.³⁵ What further separates MOFs from zeolites for H₂ gas storage is the flexible organic pores in MOFs, which can be controlled dynamically, thereby confining H₂ in the framework. This dynamic pore confinement was reported with nickel bipyridine-based MOFs.³⁶

In the field of gas separation, zeolites, typically chosen due to their high selectivity resulting from their rigid pore structure, exhibit a well-defined microporous network. MOFs, however, exhibit either rigid or flexible separation membrane characteristics. An

added advantage that MOFs have over zeolites is the tunability that MOFs exhibit by substitution of metal, change of organic ligand, or functionalization of ligand or MOF.³⁷ Examples of rigid MOF gas separation includes ZIFs 68, 69, 70 for CO₂ separation from either CO or CH₄.³⁸ Examples of flexible MOF separation include Al- and Cr- based MIL-53 and MIL-47 for CO₂ over CH₄.³⁹

In the field of heterogeneous catalysis, zeolites have been prominent in various reactions in the chemical industry. The properties of zeolites led to this popularity are high crystallinity, surface area, and thermal stability. In the petrochemical industry, it is typical to find highly endothermic reactions requiring high operating temperatures well over 573 K, a region in which MOFs typically do not have the thermal stability. As a result, it is likely MOFs are better suited to facilitate organic synthesis reactions at lower temperatures for fine chemicals. The two main active sites that arise from MOFs are the metal oxide nodes and the organic ligands. The metal oxide nodes can serve as Lewis acid sites, while the organic ligands can contain Brønsted acid sites. The inherent micropore structure of MOFs allows the possibility for reactions to take place on the external surface of the catalyst or within the pores.

Examples of MOFs studied for catalytic reactions include: HKUST-1 for aldehyde cyanosilylation reaction⁴⁰, MIL-100 (Cr,Fe) for Friedel-Crafts benzylation⁴¹, aldehyde cyanosilylation⁴², the oxidation of sulfides⁴³, Knoevenagel condensation⁴⁴ and MIL-100 for asymmetric aldol condensation⁴⁵. MOF-5 has also been studied for photocatalytic applications⁴⁶.

1.4 Motivation and thesis outlines

Compared to aluminosilicate zeolites, metal organic frameworks are a relatively new class of nanoporous materials. Since MOFs are less thermally and chemically stable than zeolites, lower temperature biomass conversion towards valuable chemicals is the most likely application for MOFs. This thesis seeks to investigate the potential for biomass conversion of sugars towards valuable organic products with UiO-66 (Universitet i Oslo 66), a novel MOF with exceptional thermal and chemical stability.

Chapter 1 of this thesis investigates the synthesis and characterization of UiO-66 catalyst to elucidate further understanding of UiO-66 structure and activity.

Chapter 2 reports on the kinetics of inulin decomposition over UiO-66 through the role and properties of UiO-66 Brønsted acid sites at lower temperatures. In this study, different kinetic models elucidate the mechanism for which UiO-66 cleaves glycosidic sugar bonds compared to random HCl and pore-mouth zeolite cleavage.

Chapter 4 of this thesis seeks to produce a valuable platform chemical, alkyl lactate, from simple sugars through a direct synthesis procedure using UiO-66. This work investigates the effect of solvent and saccharide on catalytic activity and reaction kinetics for alkyl lactate yield. Lewis acid esterification provides a route for fructose conversion to alkyl lactate. This chapter will seek to investigate the role of Lewis and Brønsted acid sites of UiO-66 towards alkyl lactate yield for different sources of sugar, including longer fructose oligomers such as inulin. Chapter 5 summarizes the conclusions of this thesis work with proposed future research related to the projects presented.

Chapter 2: UiO-66 Synthesis and Characterization

2.1 Introduction

UiO-66 is a MOF consisting of octahedron $[\text{Zr}_6\text{O}_4(\text{OH})_4]$ metal oxide nodes connected with 1,4-benzenedicarboxylate (BDC) organic linkers; its crystalline structure can be seen in Figure 2-1. UiO-66 has garnered interest for its high thermal and chemical stability compared to other MOFs⁴⁷. Since its first reported synthesis in 2008,⁴⁸ UiO-66 has shown potential for a wide range of applications including gas separation^{49,50}, energy storage^{51,52}, and catalysis^{53,54}. As a relatively new, catalyst there is still much to be understood about UiO-66 active sites. This chapter will discuss how UiO-66 was synthesized and subsequently characterized in order to provide insight on UiO-66 crystallinity, textural properties, micro porosity, and thermal stability.

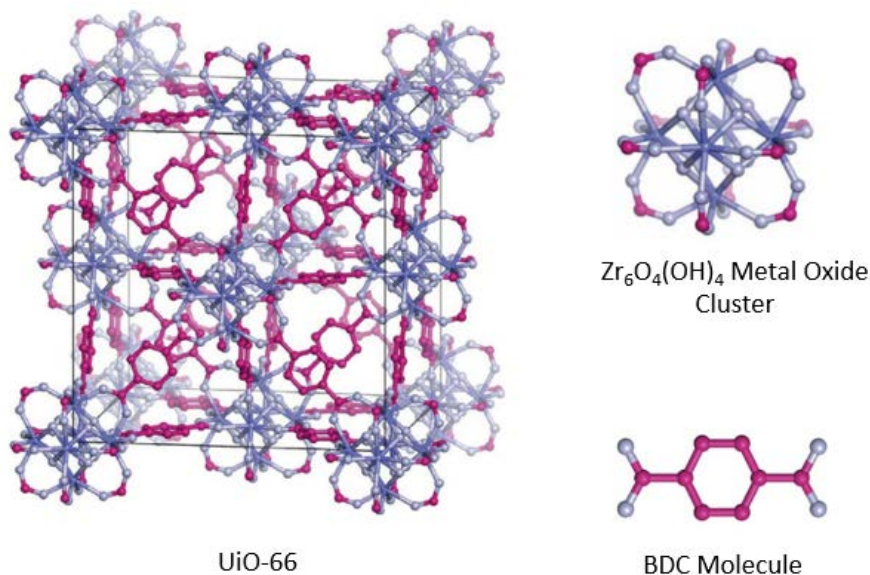


Figure 2-1. Crystalline structure of UiO-66 as well as characteristic metal oxide clusters and BDC organic linkers.⁵⁵

2.2 Experimental

2.2.1 Catalyst preparation

UiO-66 was synthesized following a reported procedure.⁴⁸ Typically, 0.106 g zirconium(IV) chloride ($ZrCl_4$, 99.9%, Alfa Aesar) and 0.068 g 1,4-benzene-dicarboxylic acid (BDC, 98%, Alfa Aesar) were dissolved in 24.9 g dimethylformamide (DMF, 99.8%, BDH) in sequence. The resultant solution was transferred into a Teflon-lined stainless steel autoclave and allowed to react at 393 K for 24 hours. The crystallized UiO-66 product was collected by centrifugation and washed by dispersing in DMF for 12 hours under rigorous magnetic stirring. The DMF washing and centrifugation steps were repeated three times. Afterwards, the UiO-66 product was dispersed in methanol solvent for 12 hours followed by centrifugation in order to remove the DMF solvent. This step was repeated two times. Finally, the UiO-66 sample was dried in a vacuum oven at 423 K overnight.

2.2.3 Catalyst characterization

Crystallinity of UiO-66 sample was determined using X-Ray Powder Diffraction (XRD) with a Bruker D8 Advance Lynx Powder Diffractometer. The textural properties of UiO-66 and BEA catalysts were determined using nitrogen (N_2) adsorption-desorption isotherm taken at 77 K with a Quantachrome instruments Autosorb-iQ Analyzer. Prior to the measurement, UiO-66 and BEA samples were degassed at 423 K and 673 K, respectively, overnight. Thermogravimetric analysis (TGA) of UiO-66 was performed using a TA Instruments TGA 2950 thermogravimetric analyzer under a mixed air and N_2 flow (1.67 mL s^{-1} , 60% air and 40% N_2) with isothermal holding at 298 K for 10 min, a heating rate of 0.050 K s^{-1} to 423 K, then a ramp rate of 0.083 K s^{-1} to 1073 K where it was

held isothermally for 10 min. Fourier-transform-IR (FT-IR) spectrum of UiO-66 was collected with a Nicolet Magna-IR 560 spectrometer in the range of 4000-600 cm^{-1} .

2.3 Results and Discussion

2.3.1 Structural and textural properties of catalyst

Figure 2-1A shows the XRD pattern of UiO-66 that was measured to understand its crystalline structure. The number of diffraction peaks and peak positions are quite similar to those reported in literature⁴⁷. This confirms the success in preparation of UiO-66 catalyst. A small peak at $2\theta = 6.2^\circ$ was observed in the pattern in Figure 2-2A. This peak can be attributed to the defects caused by missing organic linkers or clusters in certain regions of UiO-66 crystal^{56, 57}. Previous reports indicate such a peak existing in UiO-66 samples that are synthesized either at lower temperatures or with increasingly thorough sample washing after the crystallization step.^{58, 59} Figure 2-2B shows the N_2 adsorption-desorption isotherm of UiO-66. Table 2-1 summarizes the BET surface areas and pore volumes extracted from the isotherm data. The inset image in Figure 2-2B is the non-local density functional theory (NLDFT) pore size distribution of UiO-66, derived from the adsorption branch of N_2 isotherms on the basis of a spherical/cylindrical pore model. UiO-66 has two peaks centered at 8 and 10.8 Å, respectively, which correspond to the dual micropore systems, i.e., tetrahedral and octahedral cages, with sizes of 8 Å and 11 Å. Both micropore systems have a ~ 6 Å accessible windows⁶⁰, but the window size is not

measurable by N₂ isotherm for UiO-66 as the larger cavities are more prominent and distinguishable through the NLDFT method.

Figure 2-2C shows the FTIR spectrum of UiO-66 sample compared to BDC, the organic linker present in UiO-66. Carboxylic acid stretching can be seen in BDC with strong adsorption bands centered around 1300 and 1690 cm⁻¹ corresponding to C-OH symmetric stretching ($\nu_{s,C-OH}$) and C=O symmetric stretching ($\nu_{s,C=O}$). These peaks are not found in UiO-66, instead the absorption bands centered around 1400, 1590 and 1660 cm⁻¹ corresponding to the O-C-O symmetric stretching ($\nu_{s,O-C-O}$), C-C ring symmetric stretch ($\nu_{s,C-C}$), and O-C-O asymmetric stretching ($\nu_{as,O-C-O}$) vibrations are found. These characteristic vibration peaks of UiO-66 are consistent with previous reports⁶¹⁻⁶³. Evidence of Brønsted acidity can be found however in the presence of a wide adsorption band at 3200 cm⁻¹ corresponds to O-H stretching ($\nu_{s,OH}$) not found in BDC. UiO-66 stretching peaks suggest BDC is integrated into the structure but that Brønsted acidity is coming somewhere other than the carbonyl group, most likely on the metal oxide cluster. Further insight on Brønsted acidity will be explored through TGA results.

TGA measurement was done to gain insight on the thermal stability of UiO-66 sample and its Brønsted acidic properties⁶⁴. As shown in Figure 2-1D, three weight loss regions are observed in the TGA curve. The first weight loss (~7.5 wt%) took place from 298– 393 K. The sharp decrease at 393 K in the TGA curve was caused by the continuous weight loss while the temperature was kept at 393 K for 5 hours under the flowing dry air. This step removed any solvent residues in the UiO-66 sample from the synthesis. The next stage of weight loss happened at 393 - 623 K, which accounts for ~7 wt% weight loss of UiO-66 and was caused by the removal of monocarboxylate ligands and/or the

dehydroxylation of the $[\text{Zr}_6\text{O}_4(\text{OH})_4]$ cluster units.⁵³ The last weight loss step (~36.5 wt%) occurred between 623 – 800 K, corresponding to the framework decomposition of UiO-66. The TGA data in Figure 2-2D indicates that UiO-66 is thermally stable up to ~623 K.

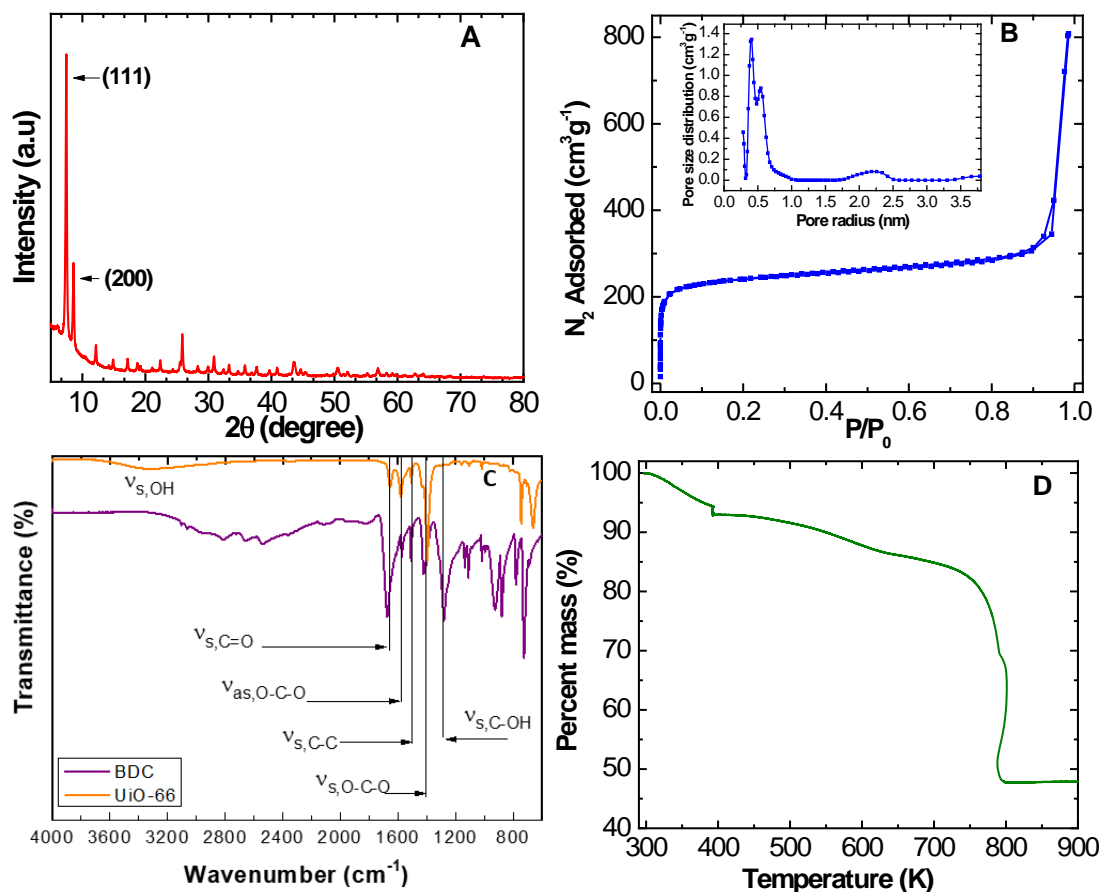


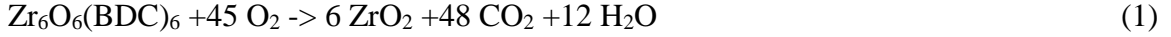
Figure 2-2. Characterization results for UiO-66 catalyst using A) wide angle XRD measurement, B) N_2 adsorption-desorption isotherms for UiO-66, C) FTIR spectroscopy for UiO-66 and BDC, and D) thermogravimetric analysis.

Table 2-1. Textural property of UiO-66 catalysts.

	S_{BET} ($\text{m}^2 \text{g}^{-1}$) ^a	S_{micro} ($\text{m}^2 \text{g}^{-1}$) ^b	V_{micro} ($\text{cm}^3 \text{g}^{-1}$) ^b	V_{total} ($\text{cm}^3 \text{g}^{-1}$) ^c
UiO-66	921	819	0.337	1.248

^a Analyzed by multi-point Brunauer–Emmett–Teller (BET) method; ^b Calculated through t-method; ^c Calculated from adsorbed volume at $p/p_0 = 0.98$.

To determine the BDC linker defects in UiO-66, the TGA data in Figure 2-1D was further analyzed according to the method reported by Shearer et al.⁵⁶. The total oxidation of UiO-66 can be represented by the following chemical reaction equation assuming the a UiO-66 unit can be represented by the (de-hydroxylated) empirical formula $Zr_6O_6(BDC)_6$ with a molar mass of 1628.03,



The theoretical TGA plateau weight of any Zr_6 MOF is therefore,

$$W_{Theo.Platt.} = \left(\frac{M_{Comp}}{M_{6 ZrO_2}} \right) W_{End} \quad (2)$$

Where M_{Comp} is the molar mass of ideal de-hydroxylated UiO-66 (1628.03 g mol⁻¹); $M_{6 ZrO_2}$ is the molar mass of 6 ZrO_2 (739.34 g mol⁻¹); and W_{end} is the end weight of TGA run (normalized to 100%),

$$W_{Theo.Platt.} = 220.2\%$$

Assuming that each missing linker is compensated by an extra oxide ion, the material is given the following average composition (where x is the number of linker deficiencies per Zr_6 unit) of $Zr_6O_{6+x}(BDC)_{6-x}$. The weight contribution per BDC linker ($Wt.PL_{Theor.}$) is the difference between the weight of the ideal de-hydroxylated material $W_{Ideal.Platt.}$ and the final weight of the sample W_{end} ; all divided by the ideal number of linkers of the Zr_6 unit ($NL_{ideal}=6$). Since W_{End} is normalized to 100%:

$$W_{Ideal.Platt.} = W_{Theo.Platt.} = 220.2\%$$

$$Wt.PL_{Theor.} = \frac{W_{Ideal.Platt.} - W_{End}}{NL_{Ideal}} \quad (3)$$

The actual experimental number of linkers ($NL_{Exp.}$) can be found by the following equation:

$$NL_{Exp} = (6 - x) = \frac{W_{Exp.Platt.} - W_{End}}{Wt.PL_{Theor.}}$$

Through, the TGA results, $W_{Exp.Platt.}$ was found at the first plateau of the TGA results at 423 K. At this point, it is assumed all desolvation, de-hydroxylation, and modulator loss has occurred. For the results, reported $W_{Exp.Platt.}$ was found to be 195%. The corresponding TGA analysis can be found in Figure 3-2. After solving for N_{LExp} , x was found to be 1.2, leading to the following average UiO-66 composition of $Zr_6O_{7.2}(BDC)_{5.8}$. This composition is indicative of an average of 1.2 missing BDC linkers per unit Zr_6 . The presence of missing linkers in UiO-66 is indicative of the presence of organic linker Brønsted acid sites.

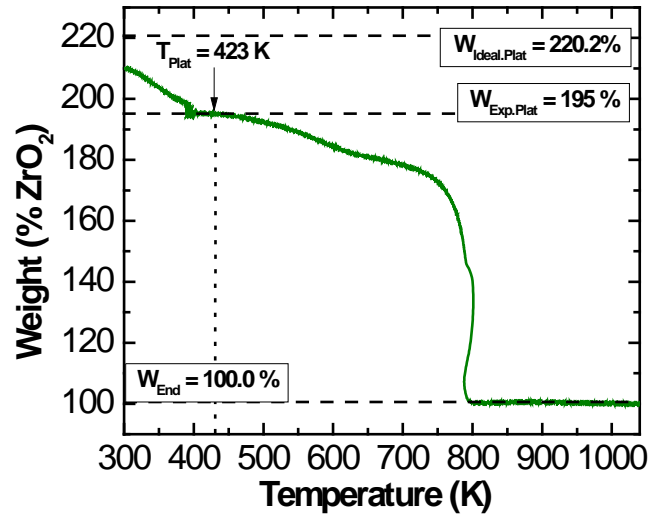


Figure 2-3. TGA graphical representation for ligand defect calculation.

2.4 Conclusions

This chapter has shown the successful synthesis of UiO-66 catalyst. Catalyst crystallinity, microporosity, and ligand functionality have been verified with conventional characterization techniques. High thermal stability, an intrinsic feature of UiO-66, has been shown with TGA results. Furthermore, quantification of missing linker defects has been presented through further TGA analysis indicating the presence of organic linker Brønsted acid sites while FTIR analysis indicates that the Brønsted acid sites are likely located on exposed metal oxide clusters and not free hanging organic ligands. In subsequent chapters, Brønsted and Lewis acidity of UiO-66 will be explored with saccharide conversion reactions.

Chapter 3: Inulin Hydrolysis on Brønsted Acid Sites in UiO-66: A Catalytic Behavior In-Between Random Chain Scission and Pore Mouth Catalysis

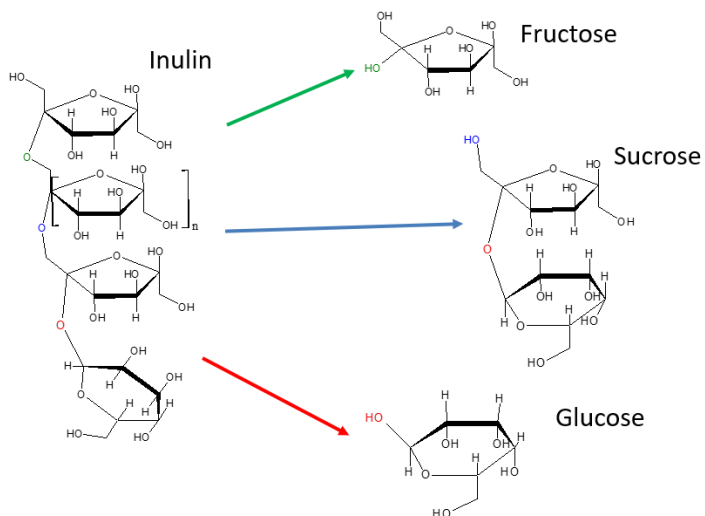
3.1 Introduction

Metal-organic frameworks (MOFs) are a class of nanoporous crystalline materials constructed from the coordination bonds between inorganic metal oxide clusters and organic ligands.^{65, 66} Due to the characteristics of high surface area, uniform micropores, tunable surface functionality and structural/mechanical flexibility, MOFs are prospected to be the next generation of important catalyst materials.⁶⁷ UiO-66 (Universitet i Oslo 66) is a zirconium-based MOF material, architected through coordination bonds between $[\text{Zr}_6\text{O}_4(\text{OH})_4]$ clusters and 1,4-benzodicarboxylic acid (BDC) struts. It is one of the most attractive MOF platforms to enabling catalysis because of the superior thermal, chemical and mechanical stability.⁴⁷ Since the first report on UiO-66 synthesis in 2008,⁴⁸ it has been explored as catalyst for a range of reactions including epoxidation of sterene oxide⁶⁸, Fischer esterification of carboxylic acids with alcohols⁶⁹, hydrolysis of the toxic nerve agents^{70, 71}, etc., in the past decade.

Despite intensive efforts on advancement of UiO-66 for catalysis^{53, 72}, the mechanistic understanding of its catalytic behaviors has not been largely explored. $[\text{Zr}_6\text{O}_4(\text{OH})_4]$ clusters and BDC struts are the construction units of UiO-66, both of which are the originating sources of active sites for catalysis. For example, the zirconium oxide (Zr_6O_8) and hydroxyls on Zr_6O_8 ^{73, 74} in the cluster nodes, the organic BDC linkers^{75, 76} and formate anions formed in the syntheses⁵⁶, or covalently bound functional groups of BDC units⁷⁷ offer diverse types of active sites for catalysis. In addition, defects caused by

missing cluster nodes and/or linkers in the framework modulate the active site accessibility and/or electronic environment, and thus the adsorption and catalytic properties of UiO-66.^{78, 79} In the past decade, UiO-66 has been primarily studied as Lewis acid catalysts for chemical transformations of simple molecular systems.^{80, 81} The exploitation of catalytic behavior of Brønsted acidity, especially for processing of complex reactant molecules such as polysaccharides, has not been attempted.

In this study, we aim to understand the catalytic properties of UiO-66 by studying inulin hydrolysis catalyzed by the Brønsted acidity. Inulin is a long, linear sugar oligomer that is comprised of repeating fructose monomers and ending with a terminal glucose monomer, often found in chicory, Jerusalem artichoke, bananas, and wheat sources^{82, 83}. The hydrolysis of inulin involves cleavage of the glycosidic bonds: the terminal glucosyl to fructosyl bond, the terminal sucrosyl to fructosyl bond, and the internal or terminal fructosyl to fructosyl.⁸⁴⁻⁸⁶ Glucose, fructose and sucrose are, therefore, the direct products in the hydrolysis process as shown in Scheme 3-1.



Scheme 3-1. Inulin hydrolysis to different saccharide products.

Heterogeneous nanoporous catalysts like zeolite have been studied as catalysts for inulin hydrolysis.^{85, 87-90} When the topology of zeolite frameworks changes from ferrierite (FER), mordenite framework inverted (MFI), beta polymorph A (BEA), mordenite (MOR), (Mobil Composition of Matter-twenty-two, MWW) to faujasite (FAU), the micropore sizes of zeolites increases, which leads to the transition of catalysis sites from external surface, to pore mouth and then in micropore.^{91, 92} A recent work by Fornefett, et al., studied the mechanism of inulin hydrolysis over a dealuminated FAU zeolite, in which an exo-enzyme like degradation behavior, i.e., a sequential splitting starting from the end of the inulin, was observed. The fructosyl chain of inulin terminates with glucose and fructose units at each end. Whether the glucose or fructose end was preferred in the exo-degradation over FAU, however, remains uncertainty. The hydrolysis of inulin in homogeneous inorganic acids, for example, aqueous HCl acid, follows the random splitting mechanism⁹³⁻⁹⁵, similar to the statistical degradation in depolymerization⁹⁶⁻⁹⁸. MOFs and zeolites are both nanoporous materials and share common characteristics such as uniform micropores and high surface areas in catalysis.^{99, 100} In UiO-66, two types of micropores (diameters of 8 and 11 Å, respectively) accessible by 6 Å windows exist.¹⁰¹ The micropore opening size of UiO-66 is quite similar to that of BEA zeolite, which consists of 12-membered ring (MR) straight channels of a free aperture of 6.6×6.7 Å viewed along the a-axis and 12-MR zigzag channels of 5.6×5.6 Å viewed along the c-axis. The MOF and zeolite materials, however, differ from the thermal/mechanical stability and structural flexibility. The zeolite is built from a more rigid inorganic aluminosilicate framework^{102, 103}, whereas the MOF is made of interconnected metal oxide and flexible organic linkers, as described above. The

difference in structure flexibility between these two materials could cause distinct catalytic consequences. In our study of catalytic behaviors of UiO-66 in inulin hydrolysis, we comparatively studied the performance of BEA in the same conditions. Moreover, the same reaction was tested in aqueous HCl acid solution. The measured reaction kinetics of inulin hydrolysis in these three catalyst systems were comparatively analyzed. Two mathematical models, Kuhn's equation and exo-enzymatic degradation that are developed for the statistical polymer splitting and sequential enzymatic catalysis, respectively, were employed to simulate the kinetics of inulin hydrolysis in UiO-66. Both models fit the kinetics data of UiO-66, while the former and later fit best for HCl acid and BEA zeolite. A catalytic behavior stays in between random chain scission and pore mouth catalysis is therefore expected for UiO-66 in inulin hydrolysis.

3.2 Experimental

3.2.1 Catalyst preparation

The synthesis of UiO-66 catalyst was carried out through the same procedure as shown in Chapter 2. The BEA zeolite was prepared from commercial zeolite beta-19 (NH_4^+ -Alfa Aesar) was activated by calcining at 923 K for 12 hours. The HCl acid was prepared using stock HCl (36% wt.) and DI water.

3.2.2 Catalyst characterization

The textural properties of UiO-66 and BEA catalysts were determined using nitrogen (N_2) adsorption-desorption isotherm taken at 77 K with a Quantachrome

instruments Autosorb-iQ Analyzer. Prior to the measurement, UiO-66 and BEA samples were degassed at 423 K and 673 K, respectively, overnight.

3.2.3 Catalyst Acidity Determination

The concentration of active Brønsted acid sites in both UiO-66 and BEA zeolite samples was determined via the reactive gas chromatography (RGC) method using isopropylamine ($\text{CH}_3\text{CH}(\text{NH}_2)\text{CH}_3$) as the probe molecule. The selective decomposition of isopropylamine ($\text{CH}_3\text{CH}(\text{NH}_2)\text{CH}_3$, 99% purity, Alfa Aesar) adsorbate on Brønsted acid site ($\text{CH}_3\text{CH}(\text{NH}_2)\text{CH}_3 \cdots \text{AlO}(\text{H})\text{Si}$) in zeolites via Hoffmann elimination forms propylene and ammonia, $\text{CH}_3\text{CH}(\text{NH}_2)\text{CH}_3 + \text{AlO}(\text{H})\text{Si} \rightarrow \text{CH}_3\text{CH}(\text{NH}_2)\text{CH}_3 \cdots \text{AlO}(\text{H})\text{Si} \rightarrow \text{CH}_2=\text{CHCH}_3 + \text{NH}_3 + \text{AlO}(\text{H})\text{Si}$.^{104, 105} The quantification of propylene by a gas chromatography (GC) instrument determined the number of Brønsted acid sites in each sample. The experimental setup and reaction conditions for chemical titration of Brønsted acid site in BEA zeolite were the same as those reported by Abdelrahman, et al.¹⁰⁵ and in our previous work.¹⁰⁶ The measurement for UiO-66 was performed at the same conditions except that the catalyst was held at 503 K in the GC inlet in the decomposition stage of adsorbates.

3.2.4 Catalytic hydrolysis of inulin

Catalytic hydrolysis of inulin (Alfa Aesar, 99% in purity) was carried out as described in our previous work.⁹¹ In a typical experiment, 20 mL DI water and 50 mg solid catalyst or 20 mL HCl acid solution (for inulin hydrolysis catalyzed by HCl) were added into a three-neck round-bottom flask (100 mL). The flask was then equipped with a reflux

condenser and heated in a temperature controlled oil bath under atmospheric pressure and magnetic stirring (1" stirring bar, 500 rpm stirring speed) conditions. After the stable reaction temperature was reached, 50 mg of inulin was added through one of the necks next to the one connected to the condenser. The initial concentration of inulin in the reactor was therefore 0.62 mM (or 2.5 g L⁻¹), which is far below the solubility (200 g L⁻¹ at room temperature). The moment that inulin was added was recorded as the reaction starting time. Liquid samples were withdrawn at regular intervals, filtered by a syringe filter, and analyzed by a high performance liquid chromatography (Agilent 1100 HPLC) equipped with a Bio-Rad Aminex HPX-87H column connected to an autosampler and a refractive index detector. Except for the desired glucose, sucrose, and fructose products, no byproduct was detected under studied reaction conditions.

3.3 Results and discussion

3.3.1 Structural and textural properties of catalysts

Figure 3-1A shows the non-local density functional theory (NLDFT) pore size distribution of UiO-66 compared with the Saito-Foley (SF) pore size distribution of BEA, both of which are derived from the adsorption branch of N₂ isotherms on the basis of a spherical/cylindrical pore model. UiO-66 has dual micropore systems with sizes of 8 Å and 11 Å, corresponding to its tetrahedral and octahedral cages, respectively (accessed by 6 Å windows)⁶⁰ BEA has micropore sizes of 5.6 x 5.6 Å and 7.7 x 6.6 Å, consistent with their topological features. The SF method shows two micropore radii centered at 5 and 6 Å, consistent with the distinct micropore channels of BEA. Figure 3-1B shows the N₂

isotherms of UiO-66, together with BEA catalyst. Table 3-1 summarized the BET surface areas and pore volumes extracted from the isotherm data. The BET surface area (S_{BET}), total pore volume (V_{total}), micropore volume (V_{micro}) and surface area (S_{micro}) of UiO-66 are higher than those of BEA.

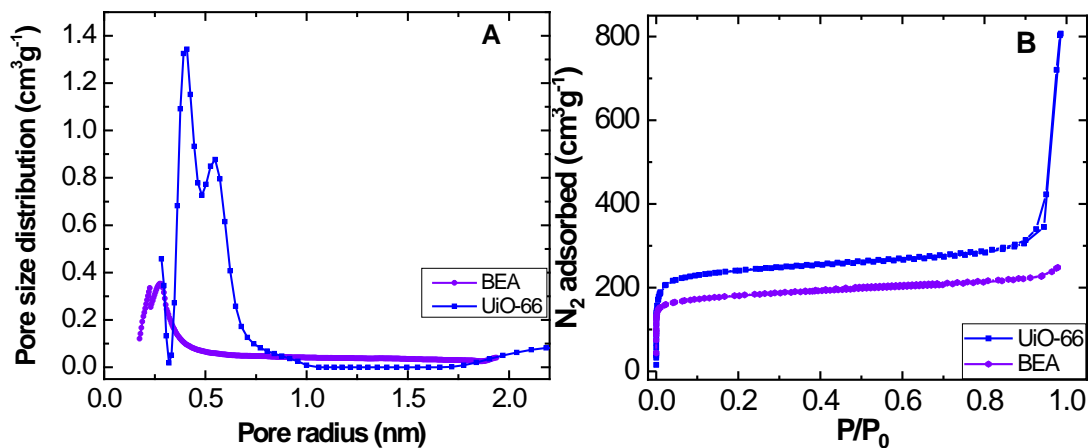


Figure 3-1. A) Pore size distributions, and B) N₂ adsorption-desorption isotherms for UiO-66 and BEA.

3.3.2 Catalyst acidity determination

The concentration of Brønsted acid sites in UiO-66 was determined by the RGC method, in which the isopropylamine ($\text{CH}_3\text{CH}(\text{NH}_2)\text{CH}_3$) was used as the probe molecule. As a basic molecule, $\text{CH}_3\text{CH}(\text{NH}_2)\text{CH}_3$ adsorbs in the zeolite and the $\text{CH}_3\text{CH}(\text{NH}_2)\text{CH}_3$ adsorbate selectively decomposes from Brønsted acid site via Hoffmann elimination into propylene and ammonia when the catalyst temperature is raised above 473 K.^{104, 105} The TGA data in Figure 3-1D shows that UiO-66 is thermally stable to ~ 623 K, beyond the decomposition temperature of $\text{CH}_3\text{CH}(\text{NH}_2)\text{CH}_3$ adsorbate. This suggests that the RGC method with $\text{CH}_3\text{CH}(\text{NH}_2)\text{CH}_3$ basic molecules can be an approach to probe the

concentration of Brønsted acid sites in UiO-66. Table 3-1 shows that UiO-66 contained $\sim 0.0881 \text{ mmol g}^{-1}$ Brønsted acid sites. The same method quantified that BEA contained $\sim 0.510 \text{ mmol g}^{-1}$ Brønsted acid sites, much higher than that of UiO-66. HCl, being a simple inorganic acid, adds Brønsted acidity throughout the aqueous solution by dissociating to H^+ and Cl^- ions. The Brønsted acid site concentration can then easily be calculated by moles of acid added to volume of water, resulting in 26.9 mmol L^{-1} .

The RGC measurement probed the presence of Brønsted acidity and its concentration in UiO-66, but the types of acidity remains elusive. Three types of Brønsted acidity, i.e., Brønsted acid molecules encapsulated within the micropores, ligated Brønsted acid groups, and covalently bound Brønsted acid functional groups of organic linking units, can possibly exist in MOFs.⁷⁶ The UiO-66 material in this study should only own the ligated Brønsted acidity since no encapsulated acid molecules or covalently bound Brønsted acid group in the BDC linkers. The ligated Brønsted acid groups can be bridging hydroxyl groups between Zr^{6+} ions, water bound to Zr^{6+} sites, or uncoordinated carboxylic acid groups of BDC due to defects. Since UiO-66 was extensively pretreated in flowing dry air at 353 K prior to the RGC measurement, the acidity due to bound water seems to be negligible. If we assume each missing BDC linker causes 1.2 defect sites (and thus acid sites) in the metal oxide cluster node, the concentration of the acid sites would be 0.72 mmol g^{-1} , higher than the Brønsted acid sites measured by the RGC method.

Overall, our acid site determination experiment confirmed the presence of Brønsted acid sites in the UiO-66 catalyst sample. We can not determine the source of these acid sites. Our control experiment, to be discussed below, for inulin hydrolysis on carboxylic acid groups in the BDC linkers showed that carboxylic acid in BDC has very low activity

than that of UiO-66. Therefore, it seems that the Brønsted acidity is mainly resulted from the bridging hydroxyl groups in the $Zr_6O_4(OH)_4$ cluster nodes. Since the inulin hydrolysis reaction took place in the aqueous solution, the water molecules bound to Zr^{6+} sites might contribute to the Brønsted acidity, but was not deemed to be as important as the bridging hydroxyl groups between Zr^{6+} ions in the RGC measurement.

Table 3-1. Textural property and acidity of BEA and UiO-66 catalysts.

	S_{BET} ($m^2 g^{-1}$) ^a	S_{micro} ($m^2 g^{-1}$) ^b	V_{micro} ($cm^3 g^{-1}$) ^b	V_{total} ($cm^3 g^{-1}$) ^c	Brønsted acid sites ($mmol g^{-1}$) ^d
UiO-66	921	819	0.337	1.248	0.0881
BEA-19	689	618	0.260	0.383	0.510

^a Analyzed by multi-point Brunauer–Emmett–Teller (BET) method; ^b Calculated through t-method; ^c Calculated from adsorbed volume at $p/p_0 = 0.98$; ^d Measured by the reactive gas chromatography method.

3.3.3 Conversion and product selectivity in inulin hydrolysis

Figure 3-2(A) shows conversion of inulin (f_{inulin} , %) versus the reaction time in the hydrolysis over the UiO-66 catalyst. For comparison, inulin conversion as a function of reaction time over BEA and in aqueous HCl acid solution are shown in Figure 3-3(B) and (C), respectively. The conversion was calculated on the basis of mono-sugar concentrations in order to account for each monosugar in inulin, as shown in Eq. (4),

$$f_{inulin} = \frac{C_{Fru} + C_{Glu} + 2C_{Suc}}{25 \times C_{Inulin}^0} \times 100\% \quad (4)$$

where, C_{Inulin}^0 is the initial inulin concentration ($mol L^{-1}$), and C_{Fru} , C_{Glu} , and C_{Suc} are the concentrations ($mol L^{-1}$) of fructose, glucose and sucrose at the local reaction time,

respectively. The digits “2” and “25” in the Eq. (1) stand for the degree of polymerization (dP) in sucrose and inulin, representative of how many monosugars are in each saccharide. The reaction was tested under each catalyst condition at four different temperatures. It should be noted that UiO-66, BEA and HCl have distinct catalytic activity, so that the reaction temperatures were selected very differently, except for 341 K, to acquire for appreciable inulin conversions. An example chromatogram of HPLC-RID spectra can be seen in Figure 3-2 showing the distinct peaks for inulin, sucrose, glucose, and fructose with retention times of 6.5, 8, 9.3, and 10.2 minutes respectively.

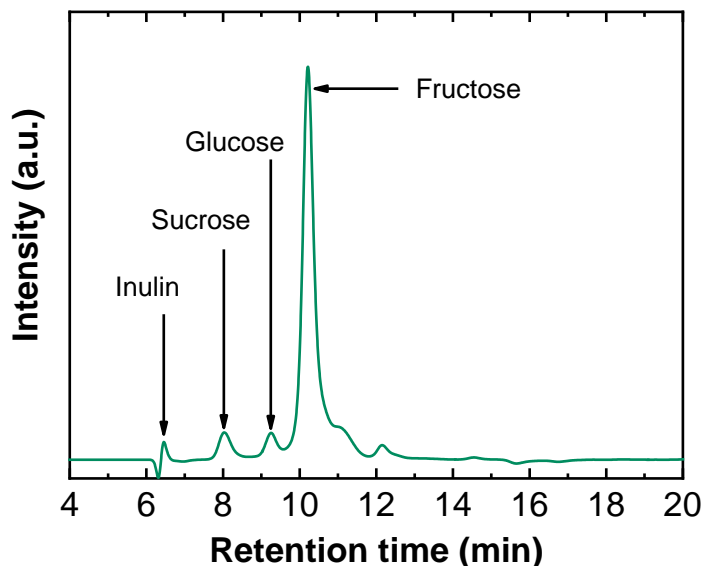


Figure 3-2. HPLC-RID chromatogram of saccharide peaks.

Overall, Figure 3-3 shows that inulin conversion curves exhibit an “S”-shape for each tested catalyst in the progress of the reaction, with depressed rate in the initial stage, increased rate with the progress, and reaching a plateau at the end. The “S”-shape behavior in the conversion curves of inulin hydrolysis is similar to those observed over cation exchanged resin¹⁰⁷, liquid acid^{108, 109} or zeolite^{91, 93} catalysts. Inulin conversion increased

with either increasing reaction temperature or time for every catalyst. At the same reaction temperature (341 K) and time, inulin conversion was much higher in UiO-66 than that of BEA or HCl acid. This indicates that UiO-66 is more active than the other control catalyst samples. In order to reach comparable inulin conversion, the reaction over BEA or HCl have to be run at a higher reaction temperature, as indicated in Figure 3-3. From the discussion on the Brønsted acid site concentration in Section 3.2 and catalyst usage quantity described in Section 2.3, the concentration of Brønsted acid sites for reactions in UiO-66, BEA and HCl acid were 0.220, 1.28 and 26.9 mM, in sequence. UiO-66 has the lowest number of Brønsted acid sites, which further indicates its highest activity among these three catalyst samples.

To understand the high catalytic activity in UiO-66, we run another control experiment by using BDC linkers directly as the catalyst. It should be noted that the concentration of BDC linkers was controlled same as those of UiO-66. The concentration of carboxylic acid groups was 30.1 mM, 137 times higher than the Brønsted acid site concentration of UiO-66 in the reaction. Figure 3-3(D) shows the conversion of inulin as a function of reaction time in the BDC solution, which is much lower (i.e., 8 times lower at the reaction temperature of 341 K and time of 240 min) than that of UiO-66. These data indicate that the uncoordinated carboxylic acid groups of the BDC linkers exposed on exterior or enclosed in micropores might not be the active sites responsible for such high activity of UiO-66. However, the partial linkage of BDC onto metal oxide clusters might strengthen its acidity than the free BDC molecules, which shows higher activity. The water molecules bound to Zr^{6+} sites or the bridging hydroxyl groups between Zr^{6+} ions might contribute to the high activity as well.

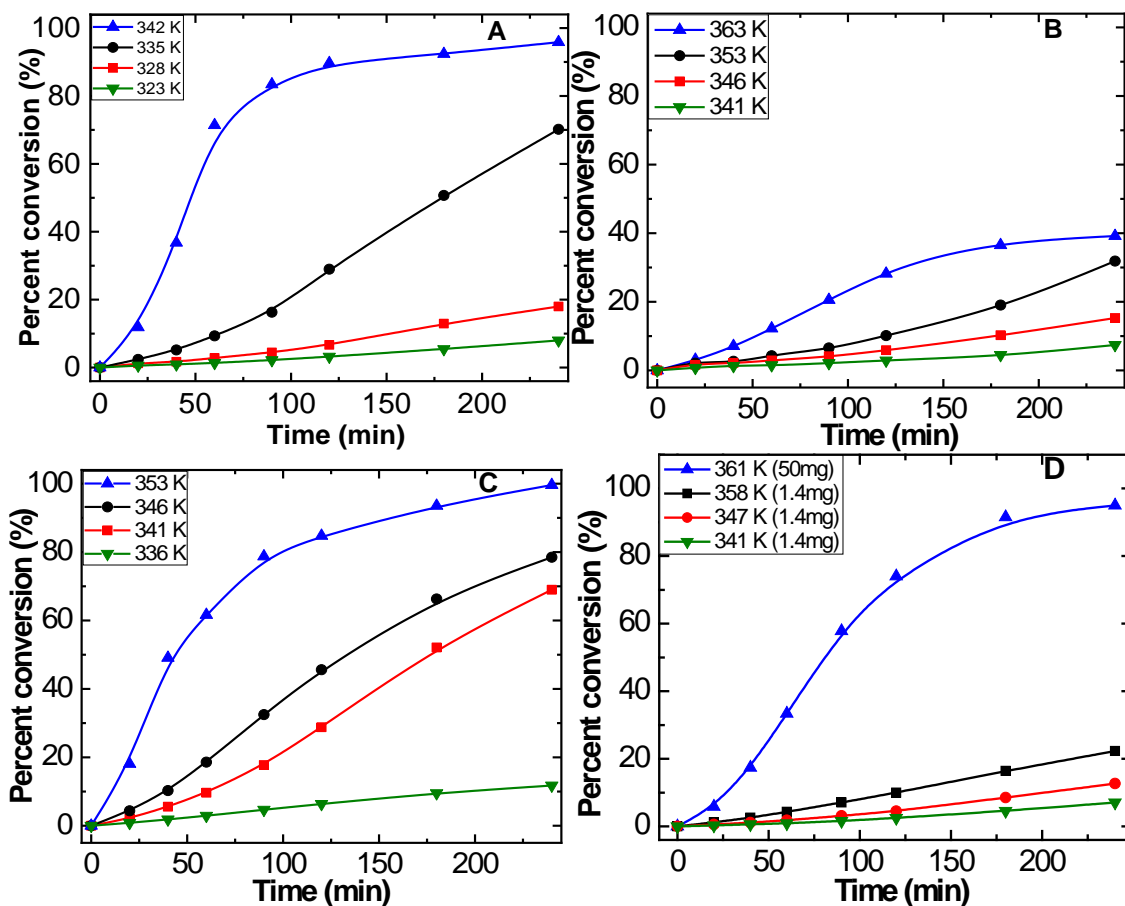


Figure 3-3. Percent conversion for inulin hydrolysis versus reaction time over A) UiO-66, B) BEA, C) HCl acid (pH of 1.57), and D) BDC acid respectively.

To understand the high catalytic activity in UiO-66, we run another control experiment by using BDC linkers directly as the catalyst. It should be noted that the concentration of BDC linkers was controlled same as those of UiO-66. The concentration of carboxylic acid groups was 30.1 mM, 137 times higher than the Brønsted acid site concentration of UiO-66 in the reaction. Figure 3-3D shows the conversion of inulin as a function of reaction time in the BDC solution, which is much lower (i.e., 8 times lower at the reaction temperature of 341 K and time of 240 min) than that of UiO-66. These data

indicate that the uncoordinated carboxylic acid groups of the BDC linkers exposed on exterior or enclosed in micropores might not be the active sites responsible for such high activity of UiO-66. However, the partial linkage of BDC onto metal oxide clusters might strengthen its acidity than the free BDC molecules, which shows higher activity. The water molecules bound to Zr^{6+} sites or the bridging hydroxyl groups between Zr^{6+} ions might contribute to the high activity as well.

There are three types of chemical bonds present in inulin: internal and terminal fructose-fructose bond, fructose-sucrose terminal bond, and fructose-glucose bond in that terminal sucrose bond. Therefore, fructose, sucrose and glucose are the primary products from the inulin hydrolysis. The analysis of the product selectivity will hint at potential catalytic pathways in the UiO-66 catalyst. Eq. (5) below defines the product selectivity from the reaction,

$$S_i = \frac{C_i}{C_{Fru} + C_{Glu} + 2C_{Suc}} \times 100\% \quad (5)$$

Where S_i is the percent selectivity for sugar “ i ” with concentration of C_i (mol L^{-1}), which can be either of fructose, glucose or sucrose. A factor of “2” was multiplied in the numerator in Eq. (2) when percent sucrose was calculated. Figure 3-4 shows the product selectivity versus conversion in inulin hydrolysis in UiO-66, BEA and HCl acid, respectively. When the inulin conversion is low (for example, $< \sim 20\%$), the product selectivity is very different among these three catalysts, while they tend to move to similar behavior with increasing conversion. In particular, in the very beginning of the reaction (i.e., differential condition, $< 5\%$ inulin conversion), BEA favored glucose formation (Figure 3-4(A)), HCl acid preferred the fructose and sucrose formation (Figure 3-4(C)), and UiO-66 (Figure 3-4(B)) had product selectivity performance in-between BEA and HCl

acid. With progress of the reaction in each of these three catalysts, the fructose selectivity monotonically increases, but the glucose selectivity has opposite trend. The sucrose selectivity follows an increasing and then decreasing trend in BEA and UiO-66 catalysts, while has monotonically decreasing trend in HCl acid. The glucose and sucrose selectivity data with HCl catalyst found in Figures 3-4(C) shows that HCl acid tends to yield higher selectivity for sucrose than glucose. This suggests that the terminal fructose-fructose bonds are weaker than the glucose-fructose bonds, likely due to the greater conformational freedom on terminal monomers than internal ones ideal for hydrolysis. This is consistent with previously reported work which found that the glucosyl-fructosyl bond was 4-5 times more resilient to cleavage than fructosyl-fructosyl bonds.¹⁰⁹ The high initial glucose cleavage and continuous fructose production suggests that inulin hydrolyzes on BEA preferably on the glucose side and then continues to cleave the fructose monomers.

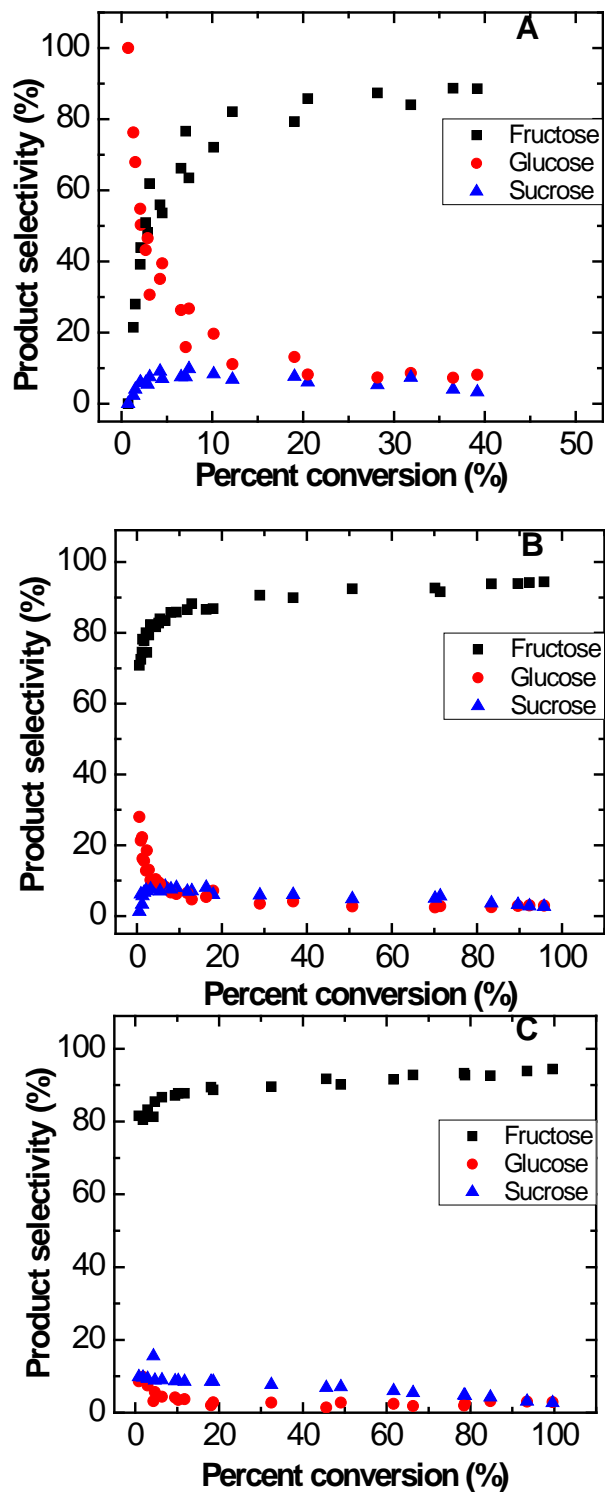


Figure 3-4. Product selectivity and conversion comparison for different catalyst conditions of A) BEA, B) UiO-66, C) HCl acid conditions for all temperature conditions.

3.3.4 Pore mouth catalysis versus random chain scission in inulin hydrolysis

In an aqueous solution, inulin does not form an extended chain structure but rather random coils. With the coiled structure, the terminal groups in the inulin chain are more labile. Therefore, they easily undergo conformation changes and accept protons onto the glycosidic bonds in the hydrolysis process.^{108, 109} Consequently, this leads to slow hydrolysis rate in the initial stage of the reaction but progressive increase in reaction rate with the reduction in degree of polymerization of the inulin chain. The “S”-shape conversion data presented in Figure 3-3 is thus expected. In comparison to the free acid sites in HCl solution, the availability of acid sites in the zeolite micropores (5.6 x 5.6 Å and 6.7 x 6.6 Å pore openings) requires the proximity and conformation of inulin in the liquid phase to the solid catalysts¹¹⁰. The molecular diameter of the terminal monosaccharides (glucose and fructose) was given as ~8.2 Å; while the terminal disaccharide (sucrose) is ~11.6 Å in diameter. Both of which are larger than BEA micropores. The randomly coiled chain of inulin in aqueous solution may limit the degree of both terminal groups penetrated into zeolite micropore channels. Therefore, the inulin hydrolysis is expected to take place preferentially on external surface and at pore mouth regions in BEA catalyst, so that a lower inulin conversion than that of HCl acid was observed at the same reaction conditions.

As a nanoporous material, UiO-66 also has two micropore systems, i.e., tetrahedral and octahedral cages, with sizes of 8 Å and 11 Å, accessible by a ~6 Å pore windows. The micropore opening size of UiO-66 is quite similar to that of BEA zeolite, but the former catalyst has distinctly higher activity than BEA and even higher than the free HCl acid in the inulin solution. Two factors could contribute to the high activity of UiO-66, i.e., the

gate effect of micropores and adaptability of flexible MOF framework structure. Thus, MOFs can take up molecules that are much larger than their pore sizes. The flexibility of the organic linkers in UiO-66 could adapt the entire catalyst to fit the conformation of inulin chain to increase its penetration into pore channels. Therefore, UiO-66 can allow entry of inulin into micropores and exit of product molecules to speed up the hydrolysis. The product selectivity data in Figure 3-3 further support these hypothesized catalytic behaviors of UiO-66 and BEA catalysts. The inulin hydrolysis in HCl aqueous solution follows the statistical splitting ⁹⁷, in which the probability of yielding fructose at the beginning of the reaction is principally higher than that of yielding glucose which is only present at the end of the polymer chain. The pore mouth catalysis in BEA apparently promoted the glucose formation. The glucose formation in UiO-66 stayed in-between BEA and HCl acid, suggests mixed effects of random chain scission and pore mouth catalysis. To further understand the in-between catalytic behavior of UiO-66, we replotted the selectivity data, glucose versus fructose (Figure 3-5A) and glucose versus sucrose (Figure 3-5B), respectively, in the course of the reaction. As shown in Figure 3-5A, the formation of glucose compared to fructose is much lower and increases significantly at the end of the reaction up to the level given by the average degree of polymerization. The solid, dark green line represents an idealized 1:24 stoichiometric molar ratio of glucose to fructose (from the degree of polymerization) in inulin used in the present study. In the case of BEA, the formation of glucose compared to fructose is much higher than of HCl solution and the stoichiometric ratio line. With the reaction progress, the ratio towards to the ratio of glucose to fructose is 1:24, the degree of polymerization obtained by the analysis of statistical splitting in homogeneous HCl solution. For UiO-66 sample, the ratio of glucose to fructose

stays between those of BEA and HCl acid, which suggests that it has a hybrid behavior of random chain scission and pore mouth catalysis.

Figure 3-5B shows the concentration change of sucrose versus fructose in inulin hydrolysis over these three catalysts. During the course of reaction, the concentration of sucrose increases and decreases, which indicates it was an intermediate product compared to the end products of fructose and glucose. Correspondingly, the concentration of sucrose over UiO-66 is the lowest, followed by HCl and then BEA.

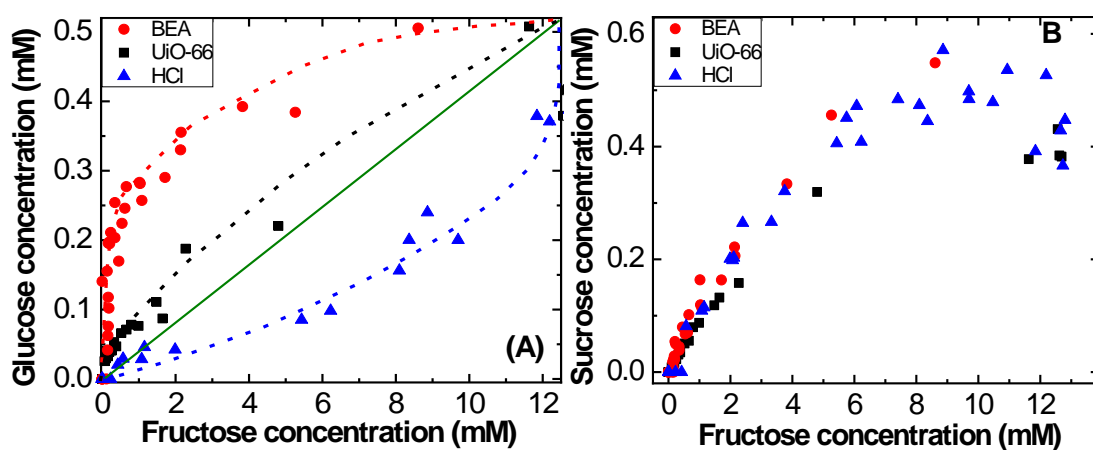


Figure 3-5. Product formation concentrations for Glucose and Fructose (A) and Sucrose and Fructose (B) for catalyst conditions of UiO-66, BEA, and HCl acid (pH 1.5-2.0).

3.3.5 Kinetic data modelling and analysis

The kinetics data discussed above suggest different catalytic behaviors exist in UiO-66, BEA and HCl acid catalyst. The random splitting following the statistic behavior is considered for inulin hydrolysis in HCl acid, pore mouth catalysis is evidenced in BEA, while an in-between hybrid random scission and pore mouth catalysis takes place in UiO-66. To further verify this understanding, we employed two mathematical models, i.e., Kuhn's and exo-enzymatic, that are developed for statistical polymer splitting and

sequential enzymatic catalysis, respectively, to simulate the kinetics of inulin hydrolysis in UiO-66.

3.3.6 Kuhn's reaction model

The Kuhn's model was proposed in the 1930's for the understanding of a statistical treatment for random polymer scission. Kuhn assumed that the polymer (of length N) was homogenous to the solution, and that all chain bonds (except for the terminal bonds) split at the same rate. Kuhn's developed this kinetic model for the acid-hydrolysis of glycogen to glucose and maltose monomers⁹⁷.

N represents the number of monomers in a chain. The probability of a bond being split is α , while the probability of a bond not being split is denoted as $(1-\alpha)$. The probability of finding a single monomer in a chain of length N, is denoted as $N\alpha^2$ because it takes two split bonds to make a single monomer. The probability of finding a chain two monomers long is thereby the probability of finding a broken chain of a polymer N long ($N\alpha^2$) multiplied by the probability of finding an unbroken monomer chain in between $(1-\alpha)$. The probability for finding a chain of two monomers in a chain N long is thereby $N\alpha^2(1-\alpha)$. The number of monomers for different chain lengths from m_1 to m_n can be expressed by the following population expression:

$$m_n = N\alpha^2(1 - \alpha)^{n-1} \quad (6)$$

The change in number of monomers for a chain length n as a function of split probability is denoted as the following:

$$\frac{dm_n}{d\alpha} = N[2\alpha(1 - \alpha)^{n-1} - (n - 1)\alpha^2(1 - \alpha)^{n-2}] \quad (7)$$

Multiplying the chain length N by the probability of a bond not being split allows the number of non-split monomers to be denoted by N' :

$$N' = N(1 - \alpha) \quad (8)$$

The split rate can therefore be defined by a first order derivative with rate constant of k_1 :

$$\frac{dN'}{dt} = k_1 N' \quad (9)$$

$$\int_N^{N'} \frac{dN'}{N'} = \int_0^t k_1 dt$$

$$N' = N e^{-k_1 t} \quad (10)$$

N' can be used to relate the split probability with the kinetic expression for splitting:

$$(1 - \alpha) = e^{-k_1 t} \quad (11)$$

$$\alpha = 1 - e^{-k_1 t}$$

$$\frac{d\alpha}{dt} = k_1 e^{-k_1 t}$$

$$d\alpha = k_1 e^{-k_1 t} dt \quad (12)$$

Equating α , $(1 - \alpha)$, and $d\alpha$ as functions of time, the change in number of monomers in a chain length n can be equated as a function of time:

$$dm_n = N[2(1 - e^{-k_1 t})(e^{-k_1 t})^{n-1} - (n - 1)(1 - e^{-k_1 t})^2(e^{-k_1 t})^{n-2}]d\alpha$$

$$dm_n = Nk_1[2(1 - e^{-k_1 t})(e^{-k_1 t})^n - (n - 1)(1 - e^{-k_1 t})^2(e^{-k_1 t})^{n-1}]dt \quad (13)$$

We are only interested in single monomer concentrations over time. Therefore, only m_1 ($n=1$) kinetics will be considered (representative of fructose or glucose indiscriminately).

$$dm_1 = 2Nk_1[(1 - e^{-k_1 t})e^{-k_1 t}]dt$$

$$dm_1 = 2Nk_1[e^{-k_1 t} - e^{-2k_1 t}]dt \quad (14)$$

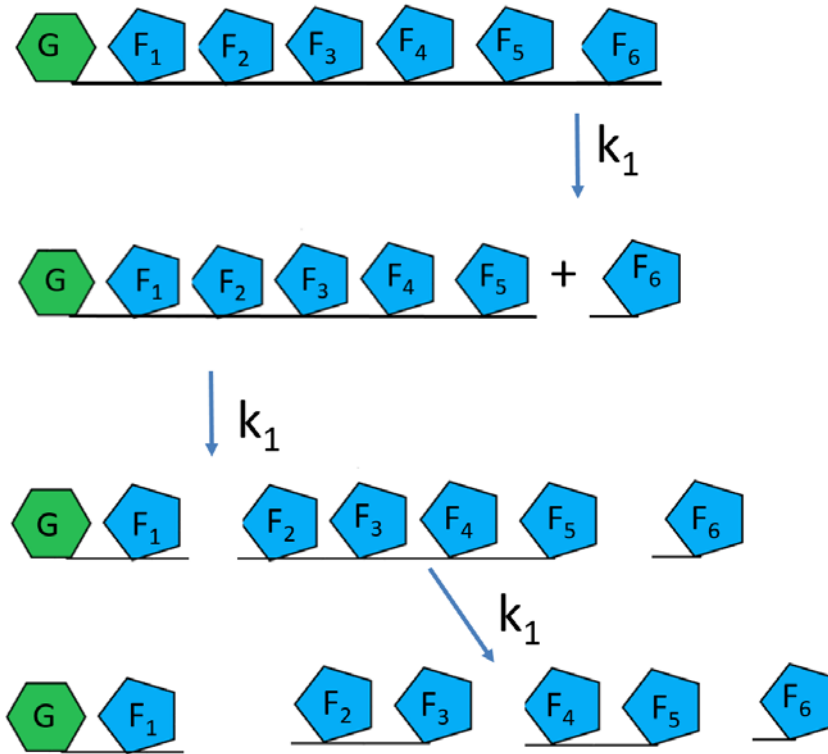
Upon further integration, the following monomer analytical expression is developed:

$$\int_0^{m_1} dm_1 = \int_0^t 2Nk_1[e^{-k_1t} - e^{-2k_1t}]dt$$

$$m_1 = N[1 - 2e^{-k_1t} + e^{-2k_1t}] \quad (15)$$

Multiplying the right-hand side of the equation with the initial concentration of Inulin produces the following derived monomer product formation (C_m , mmol L⁻¹) versus reaction time (t, min) as shown in (16),

$$C_{m_1} = NC_{I_0}[1 - 2e^{-k_1t} + e^{-2k_1t}] \quad (16)$$



Scheme 3-2. Proposed Kuhn's reaction mechanism for inulin hydrolysis via indiscriminant statistical splitting.

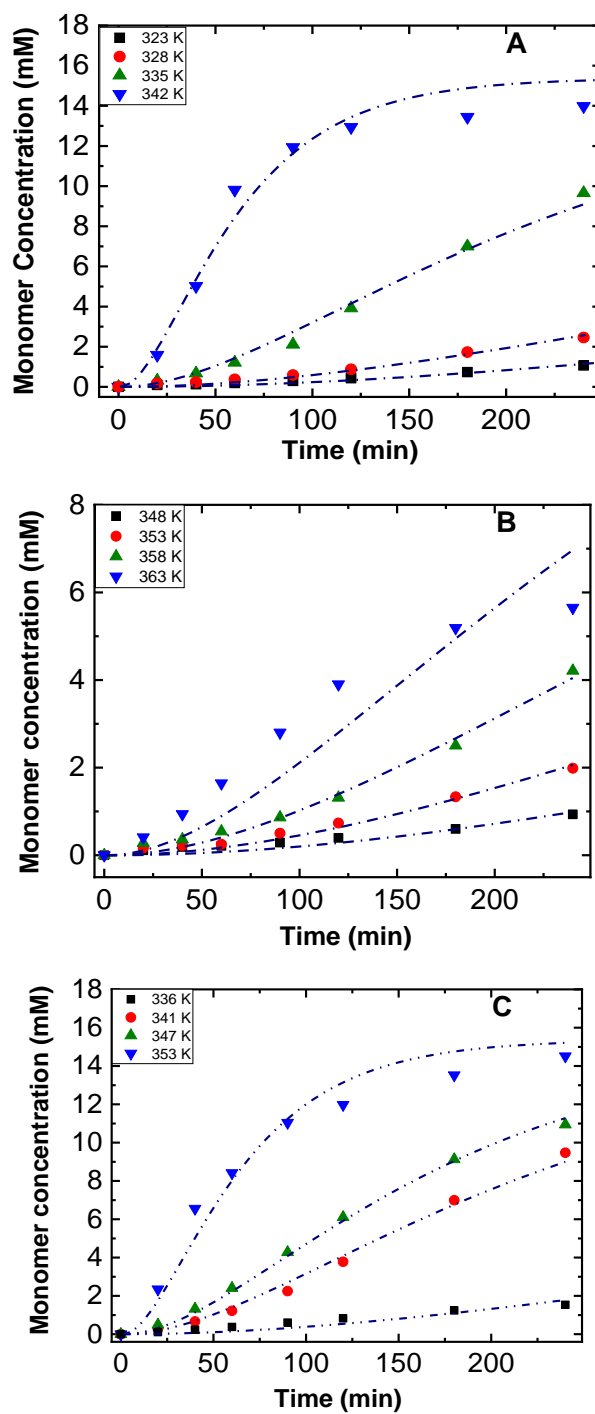


Figure 3-6. Monomer concentration versus reaction time, with Kuhn's kinetic model fitting for (A) UiO-66, (B) BEA, and (C) HCl (pH of 1.57) at different temperatures.

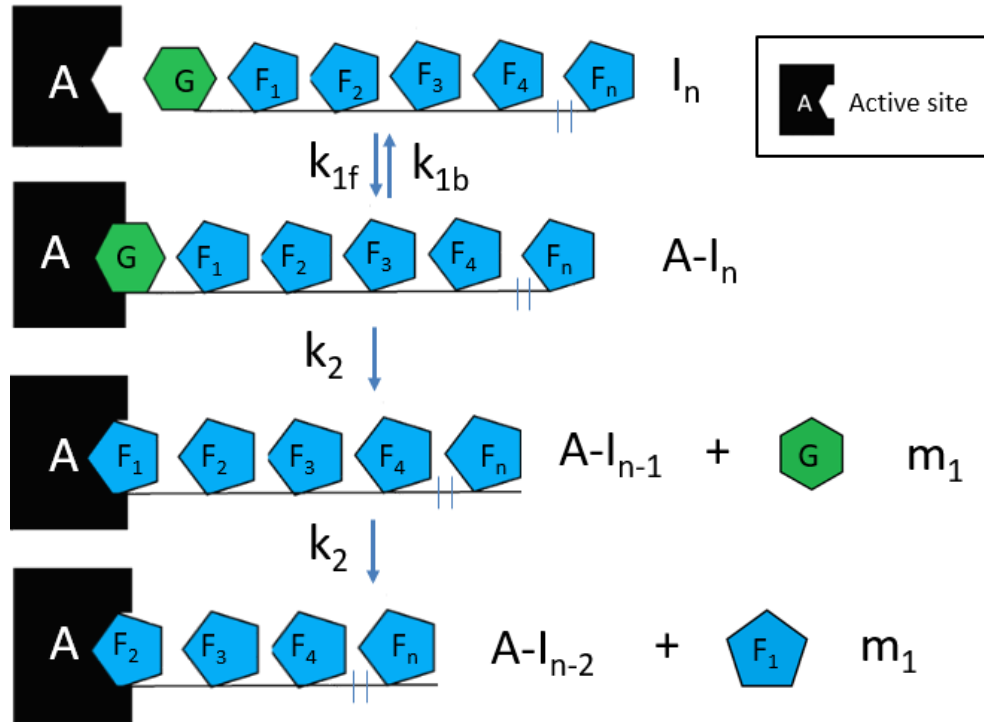
3.3.7 Exo-enzymatic model

In order to investigate if pore-mouth catalysis is the dominant reaction pathway for UiO-66 inulin hydrolysis, a novel analytical model has been proposed. Enzyme-catalyzed inulin hydrolysis is typically modeled with Michaelis-Menten kinetics^{111, 112}. Through Michaelis-Menten kinetics, there is a substrate or reactant S which bonds to an active site E, forms an enzyme substrate ES, and then releases its product P, along with a free Enzyme E. This model works well for enzymes which have high selectivity, and has been used for inulin hydrolysis with inulinase enzyme.¹¹³⁻¹¹⁵

The Michaelis-Menten equation generates a kinetic expression, where in the beginning, concentration of substrate(C_s) is high, causing linear, zeroth order product formation. The expression transitions to a first order curve as C_s decreases along the course of the reaction. This zeroth to first order conversion profile can never adequately capture the S-shaped fractional conversion curve first observed for inulin hydrolysis over strong acid and zeolite catalysts. In order to fully capture the kinetics of inulin hydrolysis, an enzyme inspired pore-mouth reaction mechanism has been proposed.

The pore sites for the catalyst can be compared to enzyme active sites. In the case of inulinase, a highly selective pocket takes in inulin and cleaves the polymer chain one at a time starting at the terminal end of the molecule^{116, 117}. To simulate this mechanism with zeolite or MOF catalyst, this exo-enzymatic model will assume that each monosugar is produced from splitting at the terminal end of the molecule inside the catalyst micropore. This assumption is reasonable since terminal fructosyl bonds in inulin have been found to be more prone to cleavage than internal fructosyl bonds, proposedly due to the change in conformation involved in hydrolysis.¹¹⁸

The reaction mechanism for inulin decomposition starts with a full inulin molecule denoted as I which is assumed to be an inulin molecule of chain length N. In this case N is assumed to be 25 from the dP of inulin from the manufacturer. M_1 represents an inulin monomer (either fructose or glucose). Inulin is a large coiled polymer, so the first step is involves a terminal monosugar attaching to the catalyst active site, denoted as A, forming a reactant-catalyst intermediate complex IA. Although inulin is comprised of a fructose chain with one terminal glucose monosugar, the reaction mechanism assumes that the reaction can be started on either the fructose end or the glucose end. The intermediate IA is then broken down to a free monosugar M_1 , a free I^{n-1} polymer chain, and a free catalyst active site A. The process then repeats itself as I^{n-1} polymer continues to be broken down to individual monosugars, eventually leading to N-monosugars. It was assumed that each monosugar was cleaved by the catalyst at the same rate K_2 . This reaction mechanism can be visualized with Scheme 3-3.



Scheme 3-3. Proposed exo-enzymatic reaction mechanism for inulin hydrolysis via pore-mouth catalysis.

The reaction mechanism is also assumed to first-order elementary reaction kinetics, yielding the following first order differential equations:

$$\frac{dC_I}{dt} = -k_1^f C_I C_A + k_1^b C_{I-A} \quad (17)$$

$$\frac{dC_{I-E}}{dt} = k_1^f C_I C_A - (k_2 + k_1^b) C_{I-A} \quad (18)$$

The pseudo steady-state assumption was made here just like in the Michaelis-Menten derivation implying that the rate of formation of the substrate-catalyst intermediate PE is equal to the rate of splitting K_2 .

$$C_{I-A} = \frac{k_1^f}{(k_1^b + k_2)} C_I C_A = K_m \quad (19)$$

Similar to the Michaelis-Menten equation, there is a parameter denoted as K_m which serves to simplify the rate expression to the following:

$$\frac{dC_{I^{n-1}-E}}{dt} = k_2 C_{I-A} - (k_1^b + k_2) C_{I^{n-1}-A} + k_1^f C_{I^{n-1}} C_A \quad (20)$$

The rate expression for the first broken down polymer-catalyst intermediate $P^{n-1}E$ is shown above. For this mechanism, k_2 was assumed to be much larger than both k_1^f and k_1^b leading to the simplified intermediate-catalyst rate expressions for each polymer chain length.

$$\frac{dC_{I^{n-1}-A}}{dt} = k_2 (C_{I-A} - C_{I^{n-1}-A}) \quad (21)$$

$$\frac{dC_{I^{n-2}-A}}{dt} = k_2 (C_{I^{n-1}-A} - C_{I^{n-2}-A}) \quad (22)$$

$$\frac{dC_{I^{n-24}-A}}{dt} = k_2 (C_{I^{n-23}-A} - C_{I^{n-24}-A}) \quad (23)$$

$$\frac{dC_{m1}}{dt} = k_2 (C_{I-A} + C_{I^{n-1}-A} + C_{I^{n-2}-A} + \dots + C_{I^{n-23}-A} + C_{I^{n-24}-A}) \quad (24)$$

The first order concentration ODEs were solved using integrating factors and yielded the following generalized expression for each polymer chain-catalyst intermediate.

$$C_{I^{n-1}-A} = K_m (1 - e^{-k_2 t}) \quad (25)$$

$$C_{I^{n-2}-A} = K_m (1 - e^{-k_2 t} (1 + k_2 t)) \quad (26)$$

$$C_{I^{n-3}-A} = K_m \left(1 - e^{-k_2 t} \left(1 + k_2 t + \frac{(k_2 t)^2}{2!} \right) \right) \quad (27)$$

$$C_{I^{n-N}-A} = K_m \left(1 - e^{-k_2 t} \left(\sum_{n=1}^N \frac{(k_2 t)^{n-1}}{(n-1)!} \right) \right) \quad (28)$$

The monosugar concentration over time was derived using a monosugar mass balance where each subsequent polymer molecule is representative of how many monosugars are produced.

$$C_{m_1}(t) = C_{I^{n-1-A}} + 2C_{I^{n-2-A}} + \dots + 24C_{I^{n-24-A}} \quad (29)$$

Combining the monosugar concentration equation over time with each individual concentration equation for each polymer-monomer intermediate, yields the following analytical equation for a polymer of N-monomers:

$$C_{m_1}(t) = K_m \left\{ \sum_{j=1}^{N-1} j - e^{-k_2 t} \sum_{j=1}^{N-1} j \sum_{n=1}^{N-1} \frac{(k_2 t)^{n-1}}{(n-1)!} \right\} \quad (30)$$

Figure 3-7 shows the exo-enzymatic model fitting each catalyst conditions at different temperatures, while Figure 3-8 compares the exo-enzymatic fitting with the Kuhn's fitting for high conversion results of each catalyst.

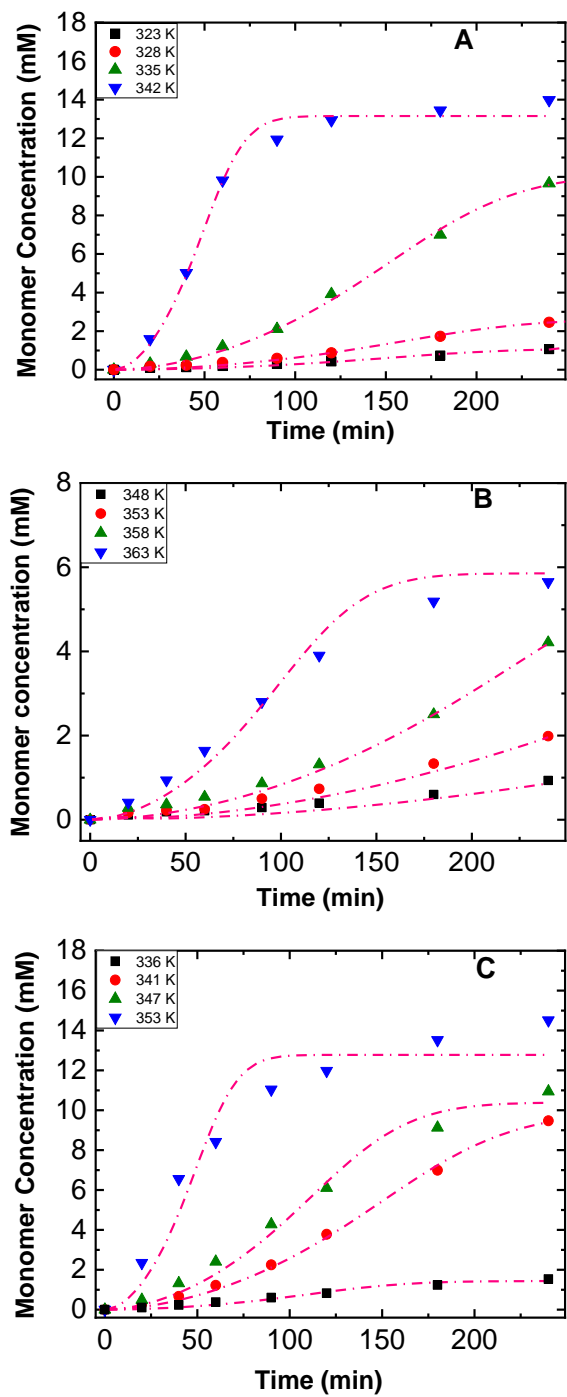


Figure 3-7. Monomer concentration versus reaction time, with Exo-Enzymatic kinetic model fitting for (A) UiO-66, (B) BEA, and (C) HCl (pH of 1.57) at different temperatures.

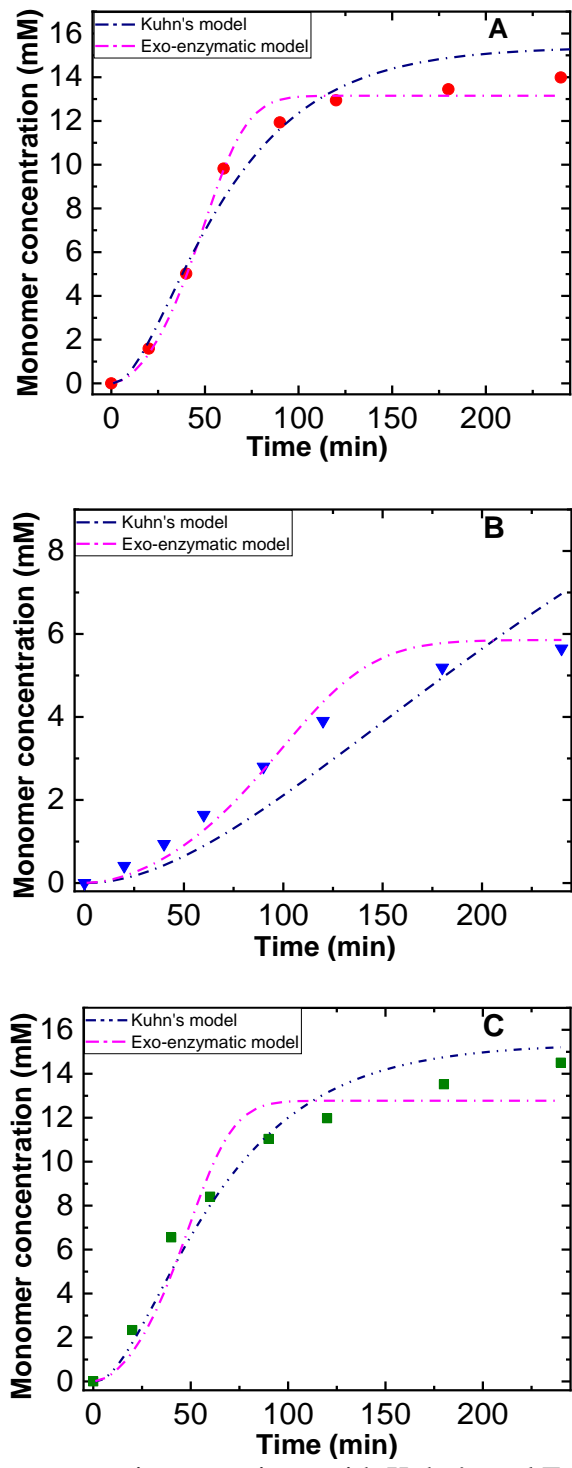


Figure 3-8. Monomer concentration over time, with Kuhn's and Exo-Enzymatic kinetic model fitting for (A) UiO-66 at 341K, (B) BEA at 363 K, and (C) HCl at 353 K (pH of 1.57)

This enzyme-inspired model proves to be good fit for all three catalyst conditions. Overall, the exo-enzymatic model shows good fitting at lower temperatures for HCl acid as seen in Figure 3-7C. However, with HCl acid conditions, Kuhn's model outperforms the exo-enzymatic model at 353K shown in Figure 3-8C. This is likely because the mechanism of HCl scission is non-discriminant cleavage along the inulin polymer that the exo-enzymatic model cannot properly capture as well.

While the exo-enzymatic model may not accurately capture random scission, it is able to capture the pore-mouth catalysis of BEA significantly better than the Kuhn's model especially at higher conversion as seen in Figure 3-8A. UiO-66 can also accurately be modeled with pore mouth catalysis through this model. By being able to fit both models well, further insight into the actual mechanism for UiO-66 is revealed.

Since UiO-66 Brønsted acidity cannot be solely responsible for its high activity, this study has shown that pore-mouth catalysis likely plays a role in this mechanism. A reason that the pore-mouth catalysis with UiO-66 outperforms BEA is that while both catalysts, can start at either terminal end of the inulin molecule, BEA has a preference for the glucose end and is significantly slower at scission than UiO-66. A reason that BEA prefers glucose to fructose could be because in inulin, fructose is found in the 5-membered ring furanose form while the terminal glucose is found in the 6-membered ring pyranose form. BEA could have a selective fitting towards cleaving 6-membered rings. The cleaving of terminal glucose also allows the possibility for the adjacent fructofuranose to isomerize to fructopyranose as suggested in previous studies¹¹⁹ which can then be cleaved itself. At the fructose end of the polymer, it is possible that BEA has to wait until the terminal fructofuranose folds into a fructopyranose to cleave. This would explain the high initial

glucose selectivity, but also the gradual buildup of sucrose from cleaving on the fructose side of smaller inulin oligomers. UiO-66, having a more flexible micropore structure, can cleave both the pyranose and furanose forms of monosugars as is demonstrated by its high catalytic activity.

Table 3-2 shows the kinetic parameters for each model and catalyst condition at different temperatures as well as the statistical goodness of fit, R^2 for each parameter. Figure 3-8 shows the Arrhenius plot of the kinetic splitting rate constants k and k_2 for the Kuhn's model and exo-enzymatic model respectively. Kuhn's model shows good fitting with the UiO-66 and HCl data well especially at higher temperatures, however it cannot fit the lower conversion data of BEA. When taking into account each of the k_2 parameters as functions of temperatures, an Arrhenius fitting for activation energy for all three catalysts (shown in Table 3-2) results in Activation energies that show that BEA outperforms HCl which outperforms UiO-66 the opposite of what is demonstrated through the conversion results. A reason for this is that Kuhn's model fails to capture lower conversion results accurately.

However, the exo-enzymatic model however, gives reasonable activation energy results in agreement with the conversion results showing activation energies of 81 kJ/mol for UiO-66; 178 kJ/mol for HCl; and 295 kJ/mol for BEA.

The exo-enzymatic model comes short however with the Brønsted acidic product distribution for sucrose. If the reaction strictly followed pore-mouth catalysis there would only be fructose and glucose products for BEA and UiO-66. For all three catalyst conditions, a maximum sucrose peak is observed. The presence of Brønsted active sites could be responsible, maximum Brønsted acid site access could be represented by HCl.

Although BEA has more Brønsted acid sites than UiO-66, only some Brønsted acid sites are on the surface as they can be found anywhere throughout the framework. It is possible that as inulin breaks down, the likelihood of non-discriminant scission by a free hanging BDC-carboxylic acid site increases. The flexible organic micropore structure could also be so efficient at pore-mouth cleavage on both sides that the rate of monomer production is high enough to be modeled by random scission. The possibility of indiscriminant Brønsted fructosyl-fructosyl or sucrosyl-fructosyl cleavage from a free hanging linker or pore-mouth terminal bond cleavage could also explain why UiO-66 has such high conversion. The hybrid scission properties of UiO-66 are confirmed with monomer-product fitting to both kinds of models. The hybrid properties are further confirmed with selectivity results which are a combination of pore-mouth high initial glucose selectivity transitioning to high fructose yields and sucrose formation found in indiscriminant Brønsted scission.

Table 3-2. Kinetic model fit parameters for Kuhn's and Exo-Enzymatic Models with R^2 values for each fit.

Catalyst	T (K)	Kuhn's model			Exo-Enzymatic model			
		k (min ⁻¹)	R^2 ^a	Activation energy (kJ·mol ⁻¹)	k_2 (min ⁻¹)	K_m (mM)	R^2 ^a	Activation energy (kJ·mol ⁻¹)
UiO-66	323	0.0014	0.9447	139	0.1208	0.0034	0.9700	81
	328	0.0023	0.9823		0.1148	0.0081	0.9880	
	335	0.0064	0.9894		0.1192	0.0313	0.9966	
	341	0.0244	0.9722		0.3663	0.4060	0.9911	
	348	0.0375	0.9679		0.5321	0.0453	0.9637	
HCl	336	0.0018	0.8457	118	0.0044	0.1621	0.9663	178
	341	0.0064	0.9921		0.1209	0.0305	0.9975	
	347	0.0085	0.9981		0.1618	0.032	0.9841	
	353	0.0233	0.9703		0.3544	0.0427	0.9381	
	358	0.0255	0.9876		0.3733	0.0428	0.9461	
BEA-19	348	0.0013	0.8660	95	0.0044	0.9144	0.7963	295
	353	0.0020	0.9766		0.0054	1.3926	0.9456	
	358	0.0032	0.9887		0.0857	0.0188	0.9861	
	363	0.0050	0.8537		0.1910	0.0167	0.9722	

^a R^2 calculated from sum-squared error and sum-squared totals of experimental data points fitted with one or two parameter kinetic models.

3.4 Conclusions

This work investigated the catalytic performance of a MOF material, i.e., UiO-66, as an effective catalyst for inulin hydrolysis. UiO-66 has been confirmed with Brønsted acidity for this reaction, although the origination of the acidity remains elusive. By comparing it to the conventional nanoporous zeolite BEA and the homogeneous inorganic HCl acid catalysts, UiO-66 has demonstrated the highest catalytic activity. The distinctly high catalytic activity could be attributed from two factors: the “gate effect” of micropores and flexibility of MOF framework structures. Both lead to the entry and exit of bulky inulin polymer into the UiO-66 micropores compared to that of BEA catalyst. The analysis on the product selectivity data elucidates the catalytic behaviors of UiO-66, which stays in-between the pore mouth catalysis and random chain scission prevalently existing in BEA and HCl acid solution. Two mathematical models, Kuhn’s statistics and exo-enzymatic, yielded the kinetics data. Both models have shown the robustness for S-shaped conversion results at lower conversion range, but differently with the progress of the reaction. The Kuhn’s model fits well for the HCl acid kinetics, exo-enzymatic fits the BEA kinetics, while UiO-66 can be modelled by both models. Both kinetics data and modelling suggests that UiO-66 has a hybrid catalytic behavior, which is consistent with its composition, and mixture of inorganic metal oxide clusters and the organic linkers.

Chapter 4: Saccharide Conversion to Lactic Acid Derivatives with Lewis and Brønsted acidic UiO-66 catalyst

4.1 Introduction

2-hydroxypropionic acid, i.e., lactic acid with a chemical formula of $\text{CH}_3\text{CH}(\text{OH})\text{COOH}$, is an important platform organic compound derived from biomass feedstock.^{120, 121} The presence of a chiral center at its second carbon and carboxylic acid group in the third carbon enable lactic acid with a lot of chemical reactivity. Therefore, a wide range of chemical transformations of lactic acid are executed to produce green solvents¹²²⁻¹²⁴, fine and commodity chemicals,¹²⁵⁻¹²⁷, fuel precursors,^{128, 129} and polylactic acid polymer.^{130, 131} In particular, the polymers derived from lactic acid are biodegradable, which have the potential to replace fossil derived plastics such as polystyrene or polyethylene terephthalate to have positive impact on the environment remedies, considering that traditional plastics are made from fossil fuel refining.¹³²

The synthesis of lactic acid has been largely and commercially practiced by a biotechnological route, i.e., fermentation.¹³³⁻¹³⁵ It is a bio-catalytic process for transformation of carbohydrate feedstocks into lactic acid by micro-organisms in aqueous solution. Mono-, di-, or polysaccharides are the main starting biomass resources. Among these, glucose and sucrose are the most important feedstock materials. Despite the success of the biotechnological process, low reaction rates, high energy consumption and large amount of waste production used in the neutralization and purification steps are the major drawbacks.^{136, 137} Alternative pathway for lactic acid production is the homogenous catalysis, in which the catalyst and reactant stay in the same phase in the conversion process. For example, the derivative of lactic acid, methyl lactate, was synthesized from hexose (glucose and fructose) and sucrose

in methanol solution in the presence of a mixture of tin chloride and sodium hydroxide ($\text{SnCl}_4\text{-NaOH}$) catalyst. SnCl_4 is the Lewis acid catalyst responsible for the hydrolysis/methanolysis steps, while NaOH neutralizes the protons generated in the reaction to increasing the product yield.³⁷ However, the homogeneous catalysts are corrosive and have a high cost and difficulty for catalyst recovery, which is not promising in large scale lactic acid production process.

In comparison to the homogeneous route, heterogeneous catalysis process that has catalyst and reactant in different phases is an attractive pathway in lactic acid production. Commonly, the reactant and/or product stays in liquid phase while catalyst is the solid in the lactic acid synthesis, so the recovery of the catalyst can be easily done by filtration, which simplifies the reaction process and reduces the operation cost. In recent years, solid catalyst materials including zeolite,^{136, 138, 139} bifunctional carbon-silica catalysts¹⁴⁰ metal oxide¹³⁶ have been explored for lactic acid synthesis. It should be noted that alkyl lactate is the direct product in most of these synthesis processes due to usage of alcohol solvent. It is more feasible to synthesize alkyl lactate through a one-step conversion of saccharides and then hydrolyze the alkyl lactate to lactic acid than it is to form lactic acid through fermentation processes. Among heterogeneous catalysts, tin-containing beta (Sn-BEA) zeolite catalyst has shown the best performance, yielding 57% methyl lactate under optimized reaction conditions, as reported by Taarning et al.¹⁴¹

Metal-organic frameworks (MOFs) are an emerging type of microporous crystalline materials. They are different from aluminosilicate zeolites as they are constructed from the coordination bonds between inorganic metal oxide ions or clusters and organic ligands^{65, 66}. High surface area, uniform micropores, tunable surface

functionality and structural/mechanical flexibility give MOFs the potential to outperform zeolites and other more traditional nanoporous catalysts.^{67, 72} . The usage of MOF materials as catalysts for production of lactic acid derivatives from biomass feedstocks has been firstly reported Murillo et al.¹⁴² In their study, methyl lactate was synthesized from glucose, fructose, and sucrose saccharides in methanol solvent at 433 K. The zeolitic imidazolate frameworks (ZIFs) and other MOFs, such as HKUST-1, MIL-53Al and MIL-101Cr, were tested for this reaction. The methyl lactate yields were 20% and 34% for sucrose on ZIF-67 and ZIF-8 respectively; yields for HKUST and MIL were found to be less than 5%. All these used MOFs have good thermal and chemical stability among a number of reported MOF structures.^{42, 143, 144}

UiO-66 is a MOF material consisting of octahedron $[\text{Zr}_6\text{O}_4(\text{OH})_4]$ metal oxide nodes connected with 1,4-benzenedicarboxylate (BDC) organic linkers.^{47, 48} It has excellent high thermal and chemical stability compared to other MOFs^{53, 72} which can be a promising heterogeneous catalyst for synthesis of lactic acid from saccharide feedstocks. Therefore, in the present work, we aim to explore the catalytic performance of UiO-66 in the catalytic synthesis of lactic acid derivatives. The effect of starting sugar, ranging from monosaccharides such as fructose and glucose, to disaccharides like sucrose and to larger sugar like inulin, on the alkyl lactate yield was studied. Methanol and ethanol, respectively, were used as the solvent to examine their effects on the reaction. The recycle capability of the catalyst was examined by repeating the catalytic reaction experiment and physicochemical property characterization. A mechanistic understanding of the reaction process over UiO-66 with both Lewis and Brønsted acid sites was discussed.

4.2 Experimental

4.2.1 Materials

ZrCl₄ (99.9%) and 1,4-benzene-dicarboxylate (BDC, 98%) were purchased from Alfa Aesar. N,N-Dimethylformamide(99.8%) was purchased from BDH; ethanol (200 proof) and methanol (100%) was purchased from Pharmco. D-Glucose(anhydrous, 99%), D-Fructose(99%), Sucrose(99%), Inulin(dP 25) was purchased from Alpha Aesar; D-Mannose(98%) was purchased from HiMedia. Methyl lactate(98%) and Ethyl lactate (98%) were purchased from TCI America. 5-Hydroxymethyl furfural(98%) was purchased from Acros Organics; 5-(Ethoxymethyl)furan-2-carboxaldehyde(97%) was purchased from Sigma Aldrich.

4.2.2 Catalytic reaction experiment

Liquid phase catalytic reactions of fructose, glucose, sucrose, and inulin in alcohol solvent were carried out in a 20 mL thick-walled glass reactor sealed with crimp tops (PTFE/silicone septum). The vessel was charged with saccharide (0.100 g), the catalyst (0.05 g), and alcohol solvent (5 mL). The glass reactor was then heated to 423 K through the use of a copper heating tube on a hot plate; the magnetic stirring was controlled at 500 rpm in all the catalysis experiments. After a certain reaction time, the reactor was quenched in an ice bath and the reaction mixture was sampled for composition analysis. A high performance liquid chromatograph (HPLC, Agilent 1100) connected to an Bio-Rad Aminex HPX-87H column connected to an autosampler and a refractive index detector to calibrate and quantify reactant and products concentration.

Samples were taken by removal of the glass test tubes and clenching in an ice bath. To insure solubility in alcohol, 0.1 g of reaction mixture was added to 0.5 grams of DI water for each sample. This dilute sample would then be filtered and prepared for analysis. The rest of the solution that was not drawn was put back into the 150 C copper cylinder to continue reaction.

Liquid samples were withdrawn at specific time intervals spanning 20 hours. During the measurement, the column was kept at 333 K with 0.005 mol L⁻¹ sulfuric acid at a flow rate of 0.6 mL min⁻¹ as the mobile phase.

The influence of external mass transfer limitations on the reaction rates was ruled out by running the reactions at a high enough stirring speed (500 rpm). In the tested reaction conditions, the absence of products from consecutive reactions of glucose and fructose was confirmed by HPLC analysis. Conversion was calculated through reactant concentrations throughout the course of the experiment quantified by HPLC compared to initial reactant concentration measured out. Percent product yield was calculated on a carbon balance based on maximum possible of alkyl lactate from each sugar (2 mol of alkyl lactate from 1 mol monosugar).

4.3 Results and discussion

4.3.1 Alkyl lactate synthesis from monosaccharides

We firstly studied the catalytic performance of UiO-66 in alkyl lactate synthesis by using monosaccharide, fructose and glucose, feedstocks. Figure 4-2 shows the conversion of each saccharide with respect to reaction time in the absence and presence of UiO-66, respectively, in either methanol or ethanol solvent. Conversion for a starting sugar of concentration of C_i^0 was defined by,

$$f_i = \left(1 - \frac{C_i}{C_i^0}\right) \times 100\% \quad (31)$$

The conversion of fructose was increased with reaction time while simultaneously outperforming the blank reaction condition. Glucose followed a similar trend, but reached full conversion much faster in methanol yet lower conversion at a faster rate in ethanol. For glucose, there is a significant change in activity for no catalyst present. Loss of reactant can be attributed to product adsorption on catalyst, however from the high reactant to catalyst mass ratio, this effect can be considered negligible.

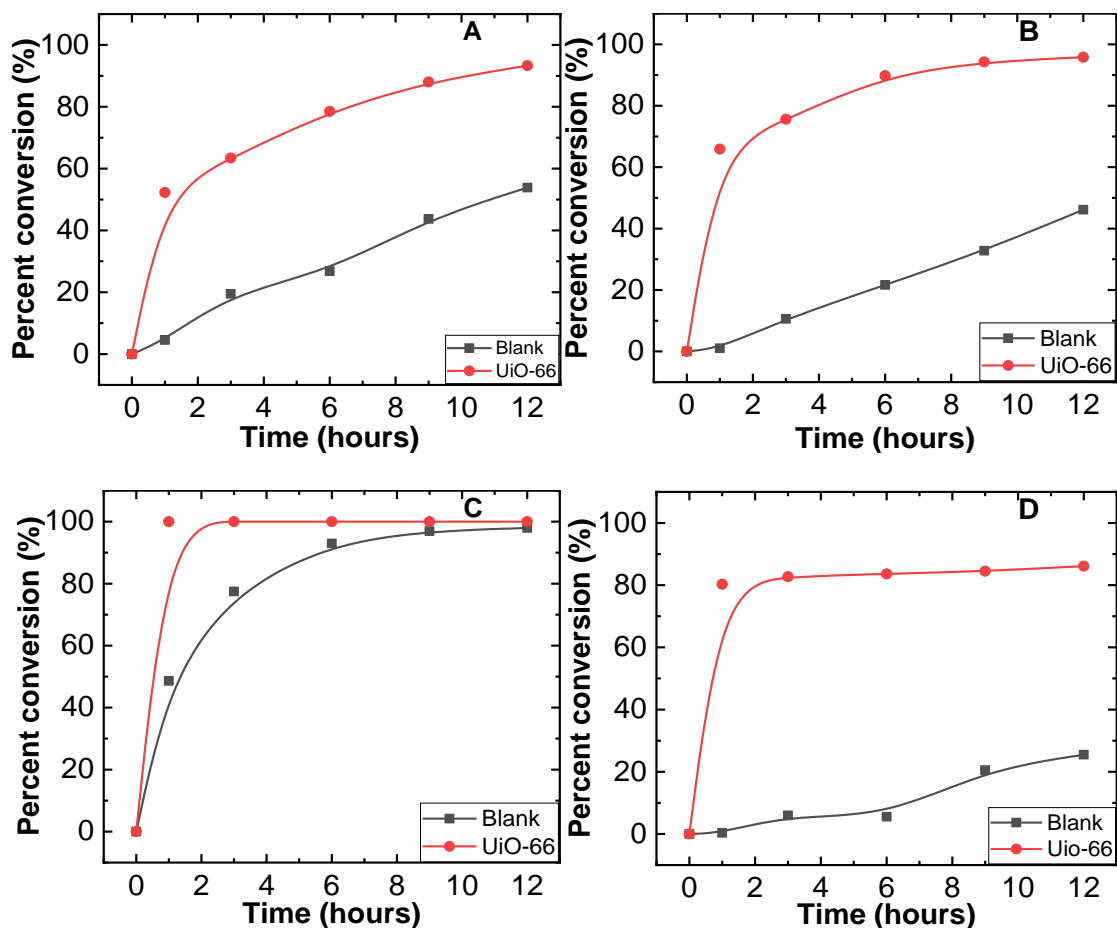


Figure 4-1. Monosugar Conversion Results for UiO-66 and no catalyst present denoted as “Blank” for fructose in methanol and ethanol (A and B) respectively; and glucose in methanol and ethanol (C and D) respectively.

High reactant conversion can come from ideally the reactant being chemically reacted to form product or in the case of sugars, it is also common at high temperatures for insoluble humin formation that agglomerate sugars and/or HMF derivatives. Since these both can occur simultaneously, an important factor in determining catalytic activity is product yield, defined for methyl lactate on a carbon basis as,

$$y^{ml} = \frac{C_{ml}(t)}{2NC_i^0} \quad (32)$$

Where N is the number of monomers in the saccharide. Since each monosaccharide can produce two alkyl lactates, alkyl lactate yields were normalized this way as sucrose (a disaccharide) could form 8 alkyl lactates; and inulin, a fructose oligomer (on average, 25 monosugars long) could form 50 alkyl lactates. The path for methyl lactate conversion is through fructose, the results for fructose product yields can be seen in Figure 4-2.

Methanol as a solvent outperforms ethanol for both catalyst conditions. Fructose to alkyl lactate conversion is directly related to Lewis acidity. It is possible that the Zr Lewis acid sites in UiO-66 have strong Lewis acid strength or that there is easy access to these sites as a result of a more flexible, organic micropore structure. With such high fructose conversion and relatively moderate to low yields of product, it is possible that fructose is converted to unidentified intermediates, side products and humins. Since there is a 4:1 mass ratio of reactant to catalyst, adsorption was not considered as a significant contribution to loss of fructose. In terms of 5-hydroxymethylfurfural (HMF) yields, there are relatively small yields (< 5%) throughout the course of the reaction, but by the 20-hour mark, the yield essentially disappears. The formation of HMF, made from Brønsted conversion of fructose, can likely be attributed to Brønsted acidity on Lewis acid sites as they can form a metal-solvent complexes. The decrease in HMF yield over time could be a result of further conversion of HMF to MMF or EMF, however insignificant yields were attained under fructose. A reason therefore for HMF consumptions could be insoluble fructose-HMF solid formation. With glucose as a reactant, there is however significant alkyl lactate yield through UiO-66 catalyst conditions (Figure 4-3).

Glucose isomerization is achieved through Lewis acid isomerization to fructose. Further Lewis acid esterification of fructose to alkyl lactate is required. A reason for higher

methyl lactate yield for glucose than for fructose could be explained by higher selectivity for pyranose (6 membered ring) glucose in MOF pores than for furanose (5- membered ring) fructose.

Glucose as a reactant causes UiO-66 to have a higher yield of fructose in the beginning of the reaction and a higher yield of mannose (an isomer of fructose and glucose) towards the end of the reaction. Different catalyst conditions appear to shift whether glucose isomerizes to either mannose or fructose. While higher fructose to mannose selectivity can shift the reaction towards fructose products.

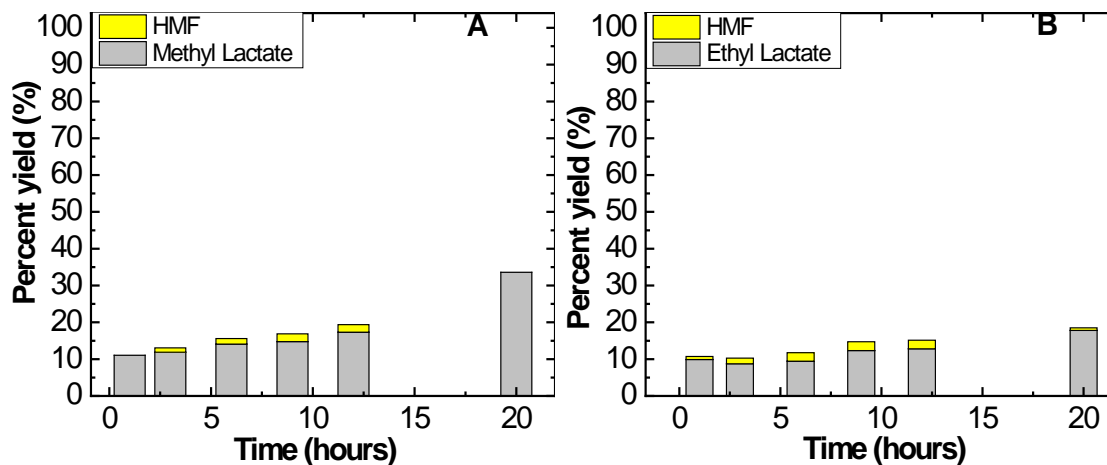


Figure 4-2. Product yield for fructose as a reactant with UiO-66 catalyst condition in (A) methanol and (B) ethanol.

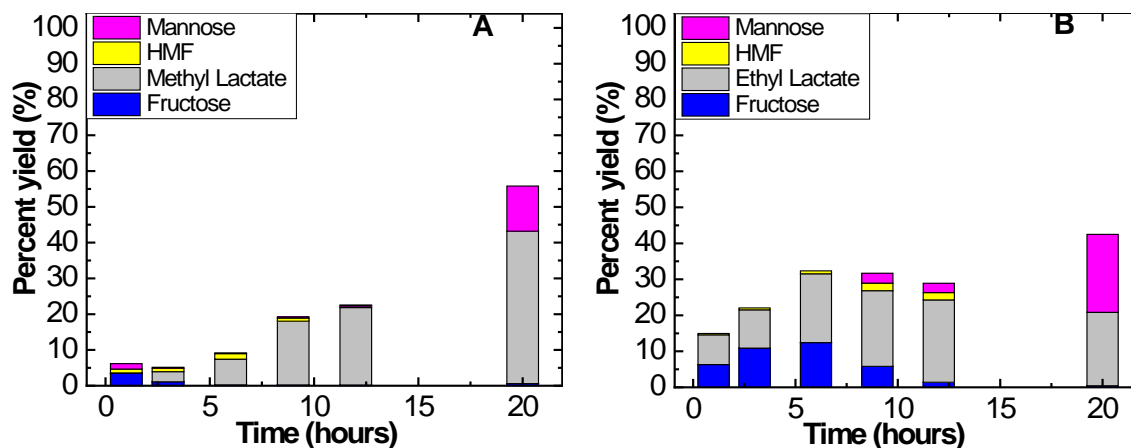


Figure 4-3. Product yield for glucose as a reactant with UiO-66 catalyst condition in (A) methanol and (B) ethanol.

4.3.3 Synthesis of alkyl lactate from disaccharide

Sucrose is a naturally abundant disaccharide consisting of one glucose hexose monomer glycosidically bonded to a fructose pentose monomer. We then studied the performance of UiO-66 in alkyl lactate synthesis from this feedstock. Like results for fructose and glucose, catalytic conversion of sucrose outperforms the same reactions without catalyst as shown in Figure 4-4. Typically, glycosidic bonds are cleaved through hydrolysis with Brønsted acidity. Based on the high conversion of sucrose, UiO-66 can use both its Lewis and Brønsted acid sites to cleave sucrose. Conversion results in both methanol and ethanol are nearly identical, this could indicate that Brønsted cleavage of sucrose has little to do with the solvent. Fructose and glucose results have indicated that Lewis acidity can be effected by choice of solvent as methanol outperformed ethanol.

The result for sucrose product yields can be found in Figure 4-5 are consistent with the glucose and fructose results with higher alkyl lactate yields in methanol than ethanol. Similar to the glucose results, there is a high initial fructose yield. Differing from the glucose results however, the mannose yield comes early in the reaction. UiO-66 has both

Lewis and Brønsted acid sites, so the Brønsted sites could be splitting fructose while Lewis acid sites simultaneously isomerize glucose to mannose and fructose to alkyl lactates. Evidence of stronger Brønsted acidity can be found by the presence of HMF throughout the course of reaction for UiO-66 for different sugars. To further understand the effect of UiO-66 Brønsted hydrolysis and Lewis esterification, inulin, a long polysaccharide will be used as a starting sugar.

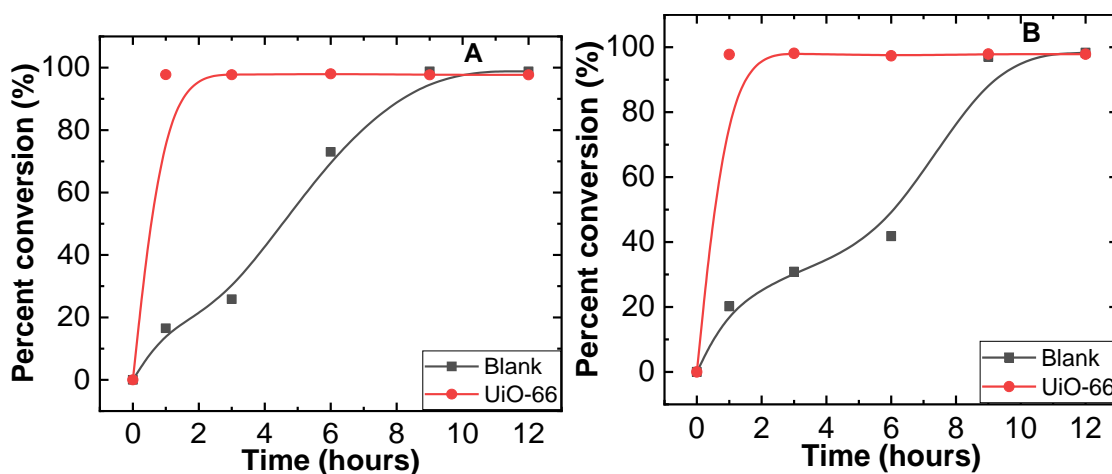


Figure 4-4. Sucrose Conversion Results for UiO-66 and no catalyst present denoted as “Blank” for fructose in methanol and ethanol (A and B) respectively.

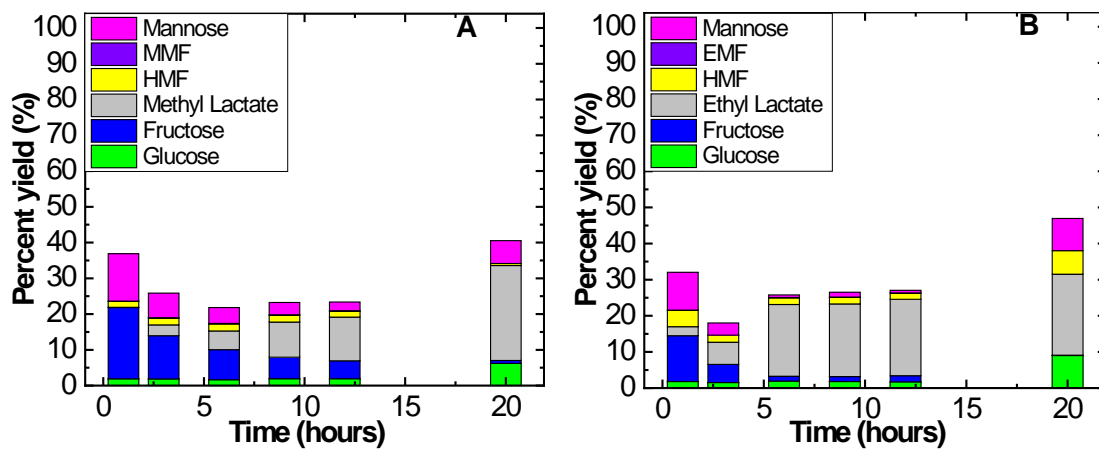


Figure 4-5. Product yield for sucrose as a reactant with UiO-66 catalyst condition in (A) methanol and (B) ethanol

4.3.4 Alkyl lactate synthesis from polymeric saccharide

Inulin is a long fructose oligomer with a terminal glucose monomer and is a representative of biomass polymer as a feedstock for alkyl lactate synthesis. Like sucrose, the monomers in inulin are connected by glycosidic O-bonds. Mannose or glucose yields early in the reaction can be indicative of terminal cleaving of inulin starting at the glucose side; while strong fructose yields can be either indicative of terminal fructose scission or random polymer scission.

Like the sucrose results, the inulin results for UiO-66 in methanol (Figure 4-6A) show high initial fructose and mannose yields. This is significant as scission in sucrose would automatically yield a fructose and glucose, while for inulin a glucose or mannose peak early in the reaction means that UiO-66 could selectively cleave towards the glucose end which would be consistent with the glucose results which have the highest yields in this study. The lack of fructose peak could indicate that inulin or broken off fructose oligomers could have a tendency towards humin formation competing with Lewis esterification towards alkyl lactate.

There is a significant difference when ethanol is used as solvent for UiO-66 catalyst. In this case there is high yield for fructose in the beginning of the reaction with glucose and glucose products being seen later towards the end of the reaction. A possible reason for this is that Brønsted cleavage is stronger with ethanol as a solvent, promoting random scission rather than pore directed cleavage. Evidence can be found by the higher presence of HMF in ethanol compared to UiO-66. As a result, inulin yields are very similar to the fructose yields for UiO-66 which makes sense as inulin is comprised almost entirely

of fructose. Higher initial yields of methyl lactate for inulin than for fructose could be attributed to inulin being able to selectively cleave both sides of inulin followed by rapid Lewis esterification. Higher initial ethyl lactate yields for fructose compared to inulin could be explained by random polymer scission or directed fructose-selective pore-mouth cleavage. Either way the initial amount of fructose is initially hampered in this case by the kinetics of inulin decomposition but ultimately reaches similar ethyl lactate yields.

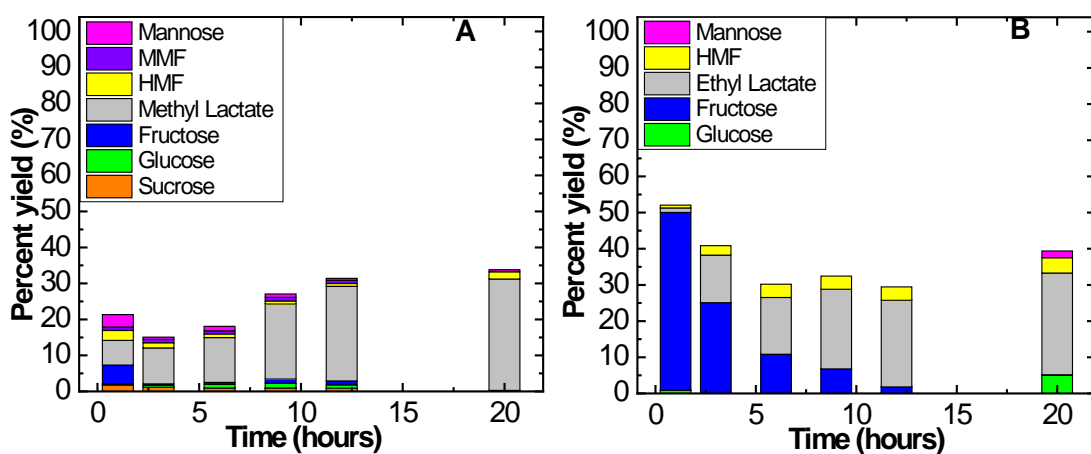


Figure 4-6. Product yields for inulin as a reactant with UiO-66 catalyst condition in (A) methanol and (B) ethanol.

4.4 Conclusions

This study sought to implement MOF material, UiO-66, as a solid catalyst for saccharide conversion into alkyl lactate, a valuable precursor of lactic acid and also biodegradable polymer. The Lewis and Brønsted acid sites existed in UiO-66 enabled the complex reaction network from saccharide for final product formation and it has flexible, organic micropores potentially allowing for larger sugars to fit through. The rate of methyl lactate formation is improved with stronger Lewis acid active sites, while HMF production is increased instead with Brønsted acid active sites. UiO-66 however shows strong selectivity for both fructose and glucose. This is likely attributed to the flexible organic pores found in UiO-66. Greater organic flexibility can lead to greater access to Lewis acid sites vastly increasing catalytic performance. UiO-66 has shown remarkable performance for biomass conversion through its flexible organic pores and Lewis and Brønsted acid sites. Biomass reactions are challenging because of all of the reaction pathways sugars can go in, the ability to fine-tune reactions conditions like starting sugars, solvent, temperature, and time are critical to maximizing yield of desired products. Using larger and cheaper sugars as carbon sources for valuable organic products is ideal for reducing carbon footprints of bio-refineries. This work has shown part of the potential that UiO-66 catalyst has for future biomass reactions, and helps to provide insight on Lewis and Brønsted acid sites in UiO-66 and their potential role for biomass conversion of sugars to lactic acid and lactic acid derivatives.

Chapter 5: Conclusions and Future Work

5.1 Conclusions

UiO-66 has shown remarkable potential for biomass conversion to valuable chemicals. In this study, UiO-66 was successfully synthesized and characterization results were implemented to gain further insight on UiO-66 structure and catalytic activity. UiO-66 Brønsted active sites were elucidated through lower temperature kinetic analysis and modeling of inulin decomposition. A novel, enzyme-inspired exo-enzymatic pore-mouth model alongside a random scission Kuhn's polymer degradation model both accurately captured monomer formation kinetics for UiO-66, suggesting that UiO-66 can utilize both mechanisms through its flexible organic framework. Selectivity results from this study suggest an initial pore-mouth preference for glucose over fructose, consistent with the Lewis acid results. Furthermore, the novel, pore-mouth model developed in this study has the potential for robust implementation in different reaction mechanisms where a terminal monomer cleavage occurs. For the first time, reactive gas chromatography was used to quantify UiO-66 Brønsted acidity and was able to show that although UiO-66 had weak Brønsted acidity compared to BEA, the flexible organic pores of UiO-66 significantly outperformed BEA for Brønsted glycosidic cleavage. UiO-66 Lewis acidity was explored through high temperature saccharide esterification with different saccharides and solvents. At the same time, UiO-66 demonstrated strong Brønsted scission of larger sugar molecules like sucrose and inulin, a long fructose oligomer. Product yields in this study indicated high, initial selectivity towards glucose and glucose isomerization products and show the potential for UiO-66 for fine chemical production from biomass.

5.2 Future work

5.2.1 Effect of Metal for Lewis Acidity in UiO-66 MOF

Lewis acidity promotes esterification of fructose towards alkyl lactate. In UiO-66, Zr (IV) metal oxide sites serve as Lewis acid sites. A way to test different metals in UiO-66 structure would be to perform a post-synthesis ion exchange of different metals such as Sn (IV) or Ti(IV) dissolved and stirred in DMF. A fully substituted Sn-UiO-66 could more closely compare to zeolite like Sn-BEA by controlling the Lewis acid metal and better investigate the role of flexible organic ligands in UiO-66 in adsorption and Lewis acid conversion. A change in metal could alter micropore diameters, possibly shifting selectivity from glucose to fructose in inulin hydrolysis.

5.2.2 Functionalization of UiO-66 for HMF Production from Cellulose

One of the advantages of MOFs is the freedom for modification through choice of organic ligand. Implementation of different Brønsted acid sites directly onto organic linkers such as BDC groups with (-HSO₃, -COOH, or -NH₃) functional groups can drastically increase Brønsted acidity of UiO-66. Lewis acid sites on UiO-66 can serve to isomerize glucose from cellulose to fructose while strong Brønsted sites can cleave cellulose to glucose and convert fructose to HMF and HMF derivatives. UiO-66 pores have already shown high glucose selectivity and high inulin decomposition activity at low temperatures.

References

1. McCusker, L. B.; Liebau, F.; Engelhardt, G., Nomenclature of structural and compositional characteristics of ordered microporous and mesoporous materials with inorganic hosts(IUPAC Recommendations 2001). In *Pure and Applied Chemistry*, **2001**; Vol. 73, p 381.
2. Shono, T.; Mingos, D. M. P.; Baghurst, D. R.; Lickiss, P. D., Novel Energy Sources for Reactions. *The New Chemistry* **2000**.
3. Bell, A. T., The impact of nanoscience on heterogeneous catalysis. *Science* **2003**, 299 (5613), 1688-1691.
4. Chorkendorff, I.; Niemantsverdriet, J. W., *Concepts of modern catalysis and kinetics*. John Wiley & Sons: **2017**.
5. Colella, C.; Gualtieri, A. F., Cronstedt's zeolite. *Microporous and Mesoporous Materials* **2007**, 105 (3), 213-221.
6. Sadeghbeigi, R., *Fluid catalytic cracking handbook: An expert guide to the practical operation, design, and optimization of FCC units*. Elsevier: **2012**.
7. Georgiev, D.; Bogdanov, B.; Angelova, K.; Markovska, I.; Hristov, Y. In *Synthetic zeolites—Structure, classification, current trends in zeolite synthesis*, **2009**.
8. Kresge, C. T.; Leonowicz, M. E.; Roth, W. J.; Vartuli, J. C.; Beck, J. S., Ordered mesoporous molecular sieves synthesized by a liquid-crystal template mechanism. *nature* **1992**, 359 (6397), 710.
9. Barrer, R. M., *Hydrothermal chemistry of zeolites*. Academic press London: **1982**; Vol. 269.
10. Kessler, H., Recent Advances in Zeolite Synthesis. In *Studies in Surface Science and Catalysis*, Elsevier: 1989; Vol. 52, pp 17-37.
11. Beck, J. S.; Vartuli, J. C.; Roth, W. J.; Leonowicz, M. E.; Kresge, C. T.; Schmitt, K. D.; Chu, C. T. W.; Olson, D. H.; Sheppard, E. W.; McCullen, S. B., A new family of mesoporous molecular sieves prepared with liquid crystal templates. *Journal of the American Chemical Society* **1992**, 114 (27), 10834-10843.
12. Bouchiba, N.; Castillo, M. L. A. G.; Bengueddach, A.; Fajula, F.; Di Renzo, F., Zeolite metastability as a function of the composition of the surrounding solution: The case of faujasite and zeolite omega. *Microporous and Mesoporous Materials* **2011**, 144 (1-3), 195-199.

13. Hoskins, B. F.; Robson, R., Design and construction of a new class of scaffolding-like materials comprising infinite polymeric frameworks of 3D-linked molecular rods. A reappraisal of the zinc cyanide and cadmium cyanide structures and the synthesis and structure of the diamond-related frameworks $[\text{N}(\text{CH}_3)_4][\text{CuI}\text{ZnII}(\text{CN})_4]$ and CuI [4, 4', 4'', 4'''-tetracyanotetraphenylmethane] $\text{BF}_4 \cdot x\text{C}_6\text{H}_5\text{NO}_2$. *Journal of the American Chemical Society* **1990**, *112* (4), 1546-1554.
14. Kitagawa, S., Metal-organic frameworks (MOFs). *Chemical Society Reviews* **2014**, *43* (16), 5415-5418.
15. Eddaoudi, M.; Moler, D. B.; Li, H.; Chen, B.; Reineke, T. M.; O'Keeffe, M.; Yaghi, O. M., Modular chemistry: secondary building units as a basis for the design of highly porous and robust metal-organic carboxylate frameworks. *Accounts of Chemical Research* **2001**, *34* (4), 319-330.
16. Rosi, N. L.; Eddaoudi, M.; Kim, J.; O'Keeffe, M.; Yaghi, O. M., Advances in the chemistry of metal-organic frameworks. *CrystEngComm* **2002**, *4* (68), 401-404.
17. Hendon, C. H.; Tiana, D.; Fontecave, M.; Sanchez, C. m.; D'arras, L.; Sassoie, C.; Rozes, L.; Mellot-Draznieks, C.; Walsh, A., Engineering the optical response of the titanium-MIL-125 metal-organic framework through ligand functionalization. *Journal of the American Chemical Society* **2013**, *135* (30), 10942-10945.
18. Chung, Y.-M.; Kim, H.-Y.; Ahn, W.-S., Friedel-Crafts acylation of p-xylene over sulfonated zirconium terephthalates. *Catalysis letters* **2014**, *144* (5), 817-824.
19. Stock, N.; Biswas, S., Synthesis of Metal-Organic Frameworks (MOFs): Routes to Various MOF Topologies, Morphologies, and Composites. *Chemical Reviews* **2012**, *112* (2), 933-969.
20. Clausen, H. F.; Poulsen, R. D.; Bond, A. D.; Chevallier, M.-A. S.; Iversen, B. B., Solvothermal synthesis of new metal organic framework structures in the zinc-terephthalic acid-dimethyl formamide system. *Journal of Solid State Chemistry* **2005**, *178* (11), 3342-3351.
21. Rabenau, A., The role of hydrothermal synthesis in preparative chemistry. *Angewandte Chemie International Edition* **1985**, *24* (12), 1026-1040.
22. Seo, Y.-K.; Yoon, J. W.; Lee, J. S.; Lee, U. H.; Hwang, Y. K.; Jun, C.-H.; Horcajada, P.; Serre, C.; Chang, J.-S., Large scale fluorine-free synthesis of hierarchically porous iron(III) trimesate MIL-100(Fe) with a zeolite MTN topology. *Microporous and Mesoporous Materials* **2012**, *157*, 137-145.
23. Tranchemontagne, D. J.; Hunt, J. R.; Yaghi, O. M., Room temperature synthesis of metal-organic frameworks: MOF-5, MOF-74, MOF-177, MOF-199, and IRMOF-0. *Tetrahedron* **2008**, *64* (36), 8553-8557.

24. Cravillon, J.; Münzer, S.; Lohmeier, S.-J.; Feldhoff, A.; Huber, K.; Wiebcke, M., Rapid Room-Temperature Synthesis and Characterization of Nanocrystals of a Prototypical Zeolitic Imidazolate Framework. *Chemistry of Materials* **2009**, *21* (8), 1410-1412.
25. Baghurst David, R. D., A new reaction vessel for accelerated syntheses using microwave dielectric super-heating effects. *Journal of the Chemical Society Dalton Transactions: Inorganic Chemistry* **1992**, (7), 1151.
26. Klinowski, J.; Paz, F. A. A.; Silva, P.; Rocha, J., Microwave-assisted synthesis of metal–organic frameworks. *Dalton Transactions* **2011**, *40* (2), 321-330.
27. Jhung, S.-H.; Lee, J.-H.; Chang, J.-S., Microwave synthesis of a nanoporous hybrid material, chromium trimesate. *Bulletin of the Korean Chemical Society* **2005**, *26* (6), 880-881.
28. Choi, J. Y.; Kim, J.; Jhung, S. H.; Kim, H.; Chang, J.; Chae, H. K., Microwave synthesis of a porous metal-organic framework, zinc terephthalate MOF-5. *BULLETIN-KOREAN CHEMICAL SOCIETY* **2006**, *27* (10), 1523.
29. Muller, U.; Putter, H.; Hesse, M.; Schubert, M.; Wessel, H.; Huff, J.; Guzmann, M.; SE, B., Method for Electrochemical Production of a Crystalline Porous Metal Organic Skeleton Material. **2007**.
30. Martinez Joaristi, A.; Juan-Alcañiz, J.; Serra-Crespo, P.; Kapteijn, F.; Gascon, J., Electrochemical Synthesis of Some Archetypical Zn²⁺, Cu²⁺, and Al³⁺ Metal Organic Frameworks. *Crystal Growth & Design* **2012**, *12* (7), 3489-3498.
31. Boldyrev, V. V.; Tkáčová, K., Mechanochemistry of solids: past, present, and prospects. *Journal of materials synthesis and processing* **2000**, *8* (3-4), 121-132.
32. Pichon, A.; Lazuen-Garay, A.; James, S. L., Solvent-free synthesis of a microporous metal–organic framework. *CrystEngComm* **2006**, *8* (3), 211-214.
33. Li, Z.-Q.; Qiu, L.-G.; Xu, T.; Wu, Y.; Wang, W.; Wu, Z.-Y.; Jiang, X., Ultrasonic synthesis of the microporous metal–organic framework Cu₃ (BTC) ₂ at ambient temperature and pressure: an efficient and environmentally friendly method. *Materials Letters* **2009**, *63* (1), 78-80.
34. Eddaoudi, M.; Li, H.; Yaghi, O. M., Highly Porous and Stable Metal–Organic Frameworks: Structure Design and Sorption Properties. *Journal of the American Chemical Society* **2000**, *122* (7), 1391-1397.
35. Morris, R. E.; Wheatley, P. S., Gas storage in nanoporous materials. *Angewandte Chemie International Edition* **2008**, *47* (27), 4966-4981.

36. Zhao, X.; Xiao, B.; Fletcher, A. J.; Thomas, K. M.; Bradshaw, D.; Rosseinsky, M. J., Hysteretic Adsorption and Desorption of Hydrogen by Nanoporous Metal-Organic Frameworks. *Science* **2004**, *306* (5698), 1012.
37. Li, J.-R.; Kuppler, R. J.; Zhou, H.-C., Selective gas adsorption and separation in metal-organic frameworks. *Chemical Society Reviews* **2009**, *38* (5), 1477-1504.
38. Banerjee, R.; Phan, A.; Wang, B.; Knobler, C.; Furukawa, H.; O'Keeffe, M.; Yaghi, O. M., High-throughput synthesis of zeolitic imidazolate frameworks and application to CO₂ capture. *Science* **2008**, *319* (5865), 939-943.
39. Bourrelly, S.; Llewellyn, P. L.; Serre, C.; Millange, F.; Loiseau, T.; Férey, G., Different Adsorption Behaviors of Methane and Carbon Dioxide in the Isotypic Nanoporous Metal Terephthalates MIL-53 and MIL-47. *Journal of the American Chemical Society* **2005**, *127* (39), 13519-13521.
40. Schlichte, K.; Kratzke, T.; Kaskel, S., Improved synthesis, thermal stability and catalytic properties of the metal-organic framework compound Cu₃ (BTC) 2. *Microporous and Mesoporous Materials* **2004**, *73* (1-2), 81-88.
41. Horcajada, P.; Surblé, S.; Serre, C.; Hong, D.-Y.; Seo, Y.-K.; Chang, J.-S.; Greneche, J.-M.; Margiolaki, I.; Férey, G., Synthesis and catalytic properties of MIL-100 (Fe), an iron (III) carboxylate with large pores. *Chemical Communications* **2007**, (27), 2820-2822.
42. Henschel, A.; Gedrich, K.; Kraehnert, R.; Kaskel, S., Catalytic properties of MIL-101. *Chemical Communications* **2008**, (35), 4192-4194.
43. Hwang, Y. K.; Hong, D.-Y.; Chang, J.-S.; Seo, H.; Yoon, M.; Kim, J.; Jung, S. H.; Serre, C.; Férey, G., Selective sulfoxidation of aryl sulfides by coordinatively unsaturated metal centers in chromium carboxylate MIL-101. *Applied Catalysis A: General* **2009**, *358* (2), 249-253.
44. Hwang, Y. K.; Hong, D. Y.; Chang, J. S.; Jung, S. H.; Seo, Y. K.; Kim, J.; Vimont, A.; Daturi, M.; Serre, C.; Férey, G., Amine grafting on coordinatively unsaturated metal centers of MOFs: consequences for catalysis and metal encapsulation. *Angewandte Chemie International Edition* **2008**, *47* (22), 4144-4148.
45. Banerjee, M.; Das, S.; Yoon, M.; Choi, H. J.; Hyun, M. H.; Park, S. M.; Seo, G.; Kim, K., Postsynthetic modification switches an achiral framework to catalytically active homochiral metal-organic porous materials. *Journal of the American Chemical Society* **2009**, *131* (22), 7524-7525.
46. Alvaro, M.; Carbonell, E.; Ferrer, B.; Llabrés i Xamena, F. X.; Garcia, H., Semiconductor Behavior of a Metal-Organic Framework (MOF). *Chemistry-A European Journal* **2007**, *13* (18), 5106-5112.

47. Kandiah, M.; Nilsen, M. H.; Usseglio, S.; Jakobsen, S.; Olsbye, U.; Tilset, M.; Larabi, C.; Quadrelli, E. A.; Bonino, F.; Lillerud, K. P., Synthesis and stability of tagged UiO-66 Zr-MOFs. *Chemistry of Materials* **2010**, *22* (24), 6632-6640.
48. Cavka, J. H.; Jakobsen, S.; Olsbye, U.; Guillou, N.; Lamberti, C.; Bordiga, S.; Lillerud, K. P., A New Zirconium Inorganic Building Brick Forming Metal Organic Frameworks with Exceptional Stability. *Journal of the American Chemical Society* **2008**, *130* (42), 13850-13851.
49. Chang, N.; Yan, X.-P., Exploring reverse shape selectivity and molecular sieving effect of metal-organic framework UiO-66 coated capillary column for gas chromatographic separation. *Journal of Chromatography A* **2012**, *1257*, 116-124.
50. Wiersum, A. D.; Soubeyrand-Lenoir, E.; Yang, Q.; Moulin, B.; Guillerm, V.; Yahia, M. B.; Bourrelly, S.; Vimont, A.; Miller, S.; Vagner, C., An evaluation of UiO-66 for gas-based applications. *Chemistry—An Asian Journal* **2011**, *6* (12), 3270-3280.
51. Jeremias, F.; Lozan, V.; Henninger, S. K.; Janiak, C., Programming MOFs for water sorption: amino-functionalized MIL-125 and UiO-66 for heat transformation and heat storage applications. *Dalton Transactions* **2013**, *42* (45), 15967-15973.
52. Tan, Y.; Zhang, W.; Gao, Y.; Wu, J.; Tang, B., Facile synthesis and supercapacitive properties of Zr-metal organic frameworks (UiO-66). *RSC Advances* **2015**, *5* (23), 17601-17605.
53. Valenzano, L.; Civalieri, B.; Chavan, S.; Bordiga, S.; Nilsen, M. H.; Jakobsen, S.; Lillerud, K. P.; Lamberti, C., Disclosing the Complex Structure of UiO-66 Metal Organic Framework: A Synergic Combination of Experiment and Theory. *Chemistry of Materials* **2011**, *23* (7), 1700-1718.
54. Yuan, Y.-P.; Yin, L.-S.; Cao, S.-W.; Xu, G.-S.; Li, C.-H.; Xue, C., Improving photocatalytic hydrogen production of metal-organic framework UiO-66 octahedrons by dye-sensitization. *Applied Catalysis B: Environmental* **2015**, *168*, 572-576.
55. Cliffe, M. J.; Wan, W.; Zou, X.; Chater, P. A.; Kleppe, A. K.; Tucker, M. G.; Wilhelm, H.; Funnell, N. P.; Coudert, F.-X.; Goodwin, A. L., Correlated defect nanoregions in a metal-organic framework. *Nature communications* **2014**, *5*, 4176.
56. Shearer, G. C.; Chavan, S.; Bordiga, S.; Svelle, S.; Olsbye, U.; Lillerud, K. P., Defect Engineering: Tuning the Porosity and Composition of the Metal-Organic Framework UiO-66 via Modulated Synthesis. *Chemistry of Materials* **2016**, *28* (11), 3749-3761.
57. Gökpınar, S.; Diment, T.; Janiak, C., Environmentally benign dry-gel conversions of Zr-based UiO metal-organic frameworks with high yield and the possibility of solvent reuse. *Dalton Transactions* **2017**, *46* (30), 9895-9900.

58. Shearer, G. C.; Chavan, S.; Ethiraj, J.; Vitillo, J. G.; Svelle, S.; Olsbye, U.; Lamberti, C.; Bordiga, S.; Lillerud, K. P., Tuned to perfection: Ironing out the defects in metal-organic framework uio-66. *Chemistry of Materials* **2014**, *26* (14), 4068-4071.
59. Jakobsen, S.; Gianolio, D.; Wragg, D. S.; Nilsen, M. H.; Emerich, H.; Bordiga, S.; Lamberti, C.; Olsbye, U.; Tilset, M.; Lillerud, K. P., Structural determination of a highly stable metal-organic framework with possible application to interim radioactive waste scavenging: Hf-UiO-66. *Physical Review B* **2012**, *86* (12), 125429.
60. Yang, Q.; Wiersum, A. D.; Llewellyn, P. L.; Guillerm, V.; Serre, C.; Maurin, G., Functionalizing porous zirconium terephthalate UiO-66 (Zr) for natural gas upgrading: a computational exploration. *Chemical Communications* **2011**, *47* (34), 9603-9605.
61. Zhu, G.; Graver, R.; Emdadi, L.; Liu, B.; Choi, K. Y.; Liu, D., Synthesis of zeolite@metal-organic framework core-shell particles as bifunctional catalysts. *RSC Advances* **2014**, *4* (58), 30673-30676.
62. Lee, H.-J.; Oh, S.-J.; Choi, J.-Y.; Kim, J. W.; Han, J.; Tan, L.-S.; Baek, J.-B., In situ synthesis of poly (ethylene terephthalate)(PET) in ethylene glycol containing terephthalic acid and functionalized multiwalled carbon nanotubes (MWNTs) as an approach to MWNT/PET nanocomposites. *Chemistry of materials* **2005**, *17* (20), 5057-5064.
63. Wen, Y.-Z.; Tong, S.-P.; Zheng, K.-F.; Wang, L.-L.; Lv, J.-Z.; Lin, J., Removal of terephthalic acid in alkalized wastewater by ferric chloride. *Journal of hazardous materials* **2006**, *138* (1), 169-172.
64. Tien-Binh, N.; Rodrigue, D.; Kaliaguine, S., In-situ cross interface linking of PIM-1 polymer and UiO-66-NH₂ for outstanding gas separation and physical aging control. *Journal of Membrane Science* **2018**, *548*, 429-438.
65. James, S. L., Metal-organic frameworks. *Chemical Society Reviews* **2003**, *32* (5), 276-288.
66. Tranchemontagne, D. J.; Mendoza-Cortés, J. L.; O’Keeffe, M.; Yaghi, O. M., Secondary building units, nets and bonding in the chemistry of metal-organic frameworks. *Chemical Society Reviews* **2009**, *38* (5), 1257-1283.
67. Li, H.; Eddaoudi, M.; O’Keeffe, M.; Yaghi, O. M., Design and synthesis of an exceptionally stable and highly porous metal-organic framework. *nature* **1999**, *402* (6759), 276.
68. Blandez, J. F.; Santiago-Portillo, A.; Navalón, S.; Giménez-Marqués, M.; Álvaro, M.; Horcajada, P.; García, H., Influence of functionalization of terephthalate linker on the catalytic activity of UiO-66 for epoxide ring opening. *Journal of Molecular Catalysis A: Chemical* **2016**, *425*, 332-339.

69. Caratelli, C.; Hajek, J.; Cirujano, F. G.; Waroquier, M.; i Xamena, F. X. L.; Van Speybroeck, V., Nature of active sites on UiO-66 and beneficial influence of water in the catalysis of Fischer esterification. *Journal of Catalysis* **2017**, *352*, 401-414.
70. Katz, M. J.; Klet, R. C.; Moon, S.-Y.; Mondloch, J. E.; Hupp, J. T.; Farha, O. K., One Step Backward Is Two Steps Forward: Enhancing the Hydrolysis Rate of UiO-66 by Decreasing [OH⁻]. *ACS Catalysis* **2015**, *5* (8), 4637-4642.
71. Mondloch, J. E.; Katz, M. J.; Isley Iii, W. C.; Ghosh, P.; Liao, P.; Bury, W.; Wagner, G. W.; Hall, M. G.; DeCoste, J. B.; Peterson, G. W., Destruction of chemical warfare agents using metal-organic frameworks. *Nature materials* **2015**, *14* (5), 512.
72. Lee, J.; Farha, O. K.; Roberts, J.; Scheidt, K. A.; Nguyen, S. T.; Hupp, J. T., Metal-organic framework materials as catalysts. *Chemical Society Reviews* **2009**, *38* (5), 1450-1459.
73. Wang, C.; Liu, X.; Chen, J. P.; Li, K., Superior removal of arsenic from water with zirconium metal-organic framework UiO-66. *Scientific reports* **2015**, *5*, 16613.
74. Ling, S.; Slater, B., Dynamic acidity in defective UiO-66. *Chemical Science* **2016**, *7* (7), 4706-4712.
75. Vermoortele, F.; Vandichel, M.; Van de Voorde, B.; Ameloot, R.; Waroquier, M.; Van Speybroeck, V.; De Vos, D. E., Electronic effects of linker substitution on Lewis acid catalysis with metal-organic frameworks. *Angewandte Chemie International Edition* **2012**, *51* (20), 4887-4890.
76. Jiang, J.; Yaghi, O. M., Brønsted acidity in metal-organic frameworks. *Chemical reviews* **2015**, *115* (14), 6966-6997.
77. Vermoortele, F.; Ameloot, R.; Vimont, A.; Serre, C.; De Vos, D., An amino-modified Zr-terephthalate metal-organic framework as an acid-base catalyst for cross-aldol condensation. *Chemical communications* **2011**, *47* (5), 1521-1523.
78. Ghosh, P.; Colón, Y. J.; Snurr, R. Q., Water adsorption in UiO-66: the importance of defects. *Chemical Communications* **2014**, *50* (77), 11329-11331.
79. Trickett, C. A.; Gagnon, K. J.; Lee, S.; Gándara, F.; Bürgi, H. B.; Yaghi, O. M., Definitive molecular level characterization of defects in UiO-66 crystals. *Angewandte Chemie International Edition* **2015**, *54* (38), 11162-11167.
80. Zhang, T.; Lin, W., Metal-Organic Frameworks for Photocatalysis. In *Metal-Organic Frameworks for Photonics Applications*, Springer: **2013**; pp 89-104.
81. Farrusseng, D.; Aguado, S.; Pinel, C., Metal-organic frameworks: opportunities for catalysis. *Angewandte Chemie International Edition* **2009**, *48* (41), 7502-7513.

82. Shoaib, M.; Shehzad, A.; Omar, M.; Rakha, A.; Raza, H.; Sharif, H. R.; Shakeel, A.; Ansari, A.; Niazi, S., Inulin: Properties, health benefits and food applications. *Carbohydrate Polymers* **2016**, *147*, 444-454.
83. Niness, K. R., Inulin and oligofructose: what are they? *The Journal of nutrition* **1999**, *129* (7), 1402S-1406s.
84. Barclay, T.; Ginic-Markovic, M.; Johnston, M. R.; Cooper, P. D.; Petrovsky, N., Analysis of the hydrolysis of inulin using real time H-1 NMR spectroscopy. *Carbohydrate Research* **2012**, *352*, 117-125.
85. Abasaheed, A. E.; Lee, Y. Y., Inulin hydrolysis to fructose by a novel catalyst. *Chemical Engineering & Technology* **1995**, *18* (6), 440-444.
86. Carniti, P.; Beltrame, P. L.; Guardione, D.; Focher, B.; Marzetti, A., Hydrolysis of inulin: A kinetic study of the reaction catalyzed by an inulinase from *Aspergillus ficuum*. *Biotechnology and Bioengineering* **1991**, *37* (6), 575-579.
87. Abasaheed, A. E.; Asif, M.; Fakeeha, A. H., Zeolite-catalyzed hydrolysis of inulin to fructose in a fluidized bed reactor. *Bioprocess Engineering* **1999**, *20* (4), 343-348.
88. Moreau, C.; Durand, R.; Duhamet, J.; Rivalier, P., Hydrolysis of fructose and glucose precursors in the presence of H-form zeolites. *Journal of Carbohydrate Chemistry* **1997**, *16* (4-5), 709-714.
89. Moreau, C.; Durand, R.; Razigade, S.; Duhamet, J.; Faugeras, P.; Rivalier, P.; Ros, P.; Avignon, G., Dehydration of fructose to 5-hydroxymethylfurfural over H-mordenites. *Applied Catalysis a-General* **1996**, *145* (1-2), 211-224.
90. Abasaheed, A. E.; Lee, Y. Y., Kinetics of inulin hydrolysis by zeolite LZ-M-8. *Hungarian Journal of Industrial Chemistry* **1996**, *24* (2), 149-153.
91. Oh, S. C.; Nguyendo, T.; He, Y.; Filie, A.; Wu, Y.; Tran, D. T.; Lee, I. C.; Liu, D., External surface and pore mouth catalysis in hydrolysis of inulin over zeolites with different micropore topologies and mesoporosities. *Catalysis Science & Technology* **2017**, *7* (5), 1153-1166.
92. He, Y.; Hoff, T. C.; Emdadi, L.; Wu, Y.; Bouraima, J.; Liu, D., Catalytic consequences of micropore topology, mesoporosity, and acidity on the hydrolysis of sucrose over zeolite catalysts. *Catalysis Science & Technology* **2014**, *4* (9), 3064-3073.
93. Fornefett, I.; Buttersack, C., Exo-enzyme like degradation of a polysaccharide by an inorganic solid acid catalyst. *Carbohydrate polymers* **2018**, *187*, 126-132.

94. Nasab, E. E.; Habibi-Rezaei, M.; Khaki, A.; Balvardi, M., Investigation on acid hydrolysis of inulin: a response surface methodology approach. *International journal of food engineering* **2009**, *5* (3).
95. Toran-Diaz, I.; Jain, V. K.; Allais, J. J.; Baratti, J., Effect of acid or enzymatic hydrolysis on ethanol production by *Zymomonas mobilis* growing on Jerusalem artichoke juice. *Biotechnology letters* **1985**, *7* (7), 527-530.
96. Montroll, E. W.; Simha, R., Theory of depolymerization of long chain molecules. *The Journal of Chemical Physics* **1940**, *8* (9), 721-726.
97. Kuhn, W., Über die kinetik des abbaues hochmolekularer ketten. *Berichte der deutschen chemischen Gesellschaft (A and B Series)* **1930**, *63* (6), 1503-1509.
98. Blatz, P. J.; Tobolsky, A. V., Note on the kinetics of systems manifesting simultaneous polymerization-depolymerization phenomena. *The journal of physical chemistry* **1945**, *49* (2), 77-80.
99. Peralta, D.; Chaplais, G. r.; Simon-Masseron, A. l.; Barthelet, K.; Chizallet, C. l.; Quoineaud, A.-A.; Pirngruber, G. D., Comparison of the behavior of metal–organic frameworks and zeolites for hydrocarbon separations. *Journal of the American Chemical Society* **2012**, *134* (19), 8115-8126.
100. Kreno, L. E.; Leong, K.; Farha, O. K.; Allendorf, M.; Van Duyne, R. P.; Hupp, J. T., Metal–organic framework materials as chemical sensors. *Chemical reviews* **2011**, *112* (2), 1105-1125.
101. Yang, Q.; Wiersum, A. D.; Jobic, H.; Guillerm, V.; Serre, C.; Llewellyn, P. L.; Maurin, G., Understanding the Thermodynamic and Kinetic Behavior of the CO₂/CH₄ Gas Mixture within the Porous Zirconium Terephthalate UiO-66(Zr): A Joint Experimental and Modeling Approach. *The Journal of Physical Chemistry C* **2011**, *115* (28), 13768-13774.
102. Szostak, R., *Molecular sieves*. Springer: **1989**.
103. Cundy, C. S.; Cox, P. A., The hydrothermal synthesis of zeolites: history and development from the earliest days to the present time. *Chemical Reviews* **2003**, *103* (3), 663-702.
104. Farneth, W. E.; Gorte, R. J., Methods for characterizing zeolite acidity. *Chemical reviews* **1995**, *95* (3), 615-635.
105. Abdelrahman, O. A.; Vinter, K. P.; Ren, L.; Xu, D.; Gorte, R. J.; Tsapatsis, M.; Dauenhauer, P. J., Simple quantification of zeolite acid site density by reactive gas chromatography. *Catalysis Science & Technology* **2017**, *7* (17), 3831-3841.

106. Bai, Y.; Wei, L.; Yang, M.; Chen, H.; Holdren, S.; Zhu, G.; Tran, D. T.; Yao, C.; Sun, R.; Pan, Y., Three-step cascade over a single catalyst: synthesis of 5-(ethoxymethyl) furfural from glucose over a hierarchical lamellar multi-functional zeolite catalyst. *Journal of Materials Chemistry A* **2018**, *6* (17), 7693-7705.
107. Kim, S. B.; Lee, Y. Y., Effect of diffusion in solid acid catalyzed inulin hydrolysis. *Applied Biochemistry and Biotechnology* **1988**, *17* (1), 55-72.
108. Szejtli, J.; Henriques, R.; Castimeira, M., The acid hydrolysis of inulin. *Acta Chim Acad Sci Hung* **1971**, *70*, 379-389.
109. Barclay, T.; Ginic-Markovic, M.; Johnston, M. R.; Cooper, P. D.; Petrovsky, N., Analysis of the hydrolysis of inulin using real time ¹H NMR spectroscopy. *Carbohydrate Research* **2012**, *352*, 117-125.
110. Buttersack, C.; Rudolph, H.; Mahrholz, J.; Buchholz, K., High specific interaction of polymers with the pores of hydrophobic zeolites. *Langmuir* **1996**, *12* (13), 3101-3106.
111. Michaelis, L.; Menten, M. L., The kinetics of the inversion effect. *Biochem. Z* **1913**, *49*, 333-369.
112. Johnson, K. A.; Goody, R. S., The original Michaelis constant: translation of the 1913 Michaelis–Menten paper. *Biochemistry* **2011**, *50* (39), 8264-8269.
113. Mazutti, M.; Ceni, G.; Di Luccio, M.; Treichel, H., Production of inulinase by solid-state fermentation: effect of process parameters on production and preliminary characterization of enzyme preparations. *Bioprocess and Biosystems Engineering* **2007**, *30* (5), 297-304.
114. Rouwenhorst, R. J.; Visser, L. E.; Van Der Baan, A. A.; Scheffers, W. A.; Van Dijken, J. P., Production, distribution, and kinetic properties of inulinase in continuous cultures of *Kluyveromyces marxianus* CBS 6556. *Applied and environmental microbiology* **1988**, *54* (5), 1131-1137.
115. Pessoni, R. A. B.; Figueiredo-Ribeiro, R. C. L.; Braga, M. R., Extracellular inulinases from *Penicillium janczewskii*, a fungus isolated from the rhizosphere of *Vernonia herbacea* (Asteraceae). *Journal of applied microbiology* **1999**, *87* (1), 141-147.
116. Nagem, R. A. P.; Rojas, A. L.; Golubev, A. M.; Korneeva, O. S.; Eneyskaya, E. V.; Kulminskaya, A. A.; Neustroev, K. N.; Polikarpov, I., Crystal structure of exo-inulinase from *Aspergillus awamori*: the enzyme fold and structural determinants of substrate recognition. *Journal of molecular biology* **2004**, *344* (2), 471-480.
117. Basso, A.; Spizzo, P.; Ferrario, V.; Knapic, L.; Savko, N.; Braiuca, P.; Ebert, C.; Ricca, E.; Calabro, V.; Gardossi, L., Endo- and exo-inulinases: Enzyme-substrate interaction and rational immobilization. *Biotechnology progress* **2010**, *26* (2), 397-405.

118. Barclay, T.; Ginic-Markovic, M.; Cooper, P.; Petrovsky, N., Inulin-a versatile polysaccharide with multiple pharmaceutical and food chemical uses. *Journal of Excipients and Food Chemicals* **2016**, *1* (3).
119. Christian, T. J.; Manley-Harris, M.; Field, R. J.; Parker, B. A., Kinetics of formation of di-d-fructose dianhydrides during thermal treatment of inulin. *Journal of agricultural and food chemistry* **2000**, *48* (5), 1823-1837.
120. Abdel-Rahman, M. A.; Tashiro, Y.; Sonomoto, K., Lactic acid production from lignocellulose-derived sugars using lactic acid bacteria: overview and limits. *Journal of biotechnology* **2011**, *156* (4), 286-301.
121. Danner, H.; Braun, R., Biotechnology for the production of commodity chemicals from biomass. *Chemical Society Reviews* **1999**, *28* (6), 395-405.
122. Datta, R.; Henry, M., Lactic acid: recent advances in products, processes and technologies—a review. *Journal of Chemical Technology & Biotechnology: International Research in Process, Environmental & Clean Technology* **2006**, *81* (7), 1119-1129.
123. Datta, R.; Tsai, S.-P.; Bonsignore, P.; Moon, S.-H.; Frank, J. R., Technological and economic potential of poly (lactic acid) and lactic acid derivatives. *FEMS microbiology reviews* **1995**, *16* (2-3), 221-231.
124. Henneberry, M.; Snively, J. A.; Vasek, G. J.; Datta, R., Biosolvent composition of lactate ester and D-limonene with improved cleaning and solvating properties. Google Patents: **2004**.
125. Gruber, P. R.; Hall, E. S.; Kolstad, J. J.; Iwen, M. L.; Benson, R. D.; Borchardt, R. L., Continuous process for the manufacture of a purified lactide from esters of lactic acid. Google Patents: **1993**.
126. Yuksel, A.; Sasaki, M.; Goto, M., Electrolysis reaction pathway for lactic acid in subcritical water. *Industrial & Engineering Chemistry Research* **2010**, *50* (2), 728-734.
127. Della Pina, C.; Falletta, E.; Rossi, M., A green approach to chemical building blocks. The case of 3-hydroxypropanoic acid. *Green chemistry* **2011**, *13* (7), 1624-1632.
128. Serrano-Ruiz, J. C.; Dumesic, J. A., Catalytic upgrading of lactic acid to fuels and chemicals by dehydration/hydrogenation and C–C coupling reactions. *Green Chemistry* **2009**, *11* (8), 1101-1104.
129. Bozell, J. J.; Petersen, G. R., Technology development for the production of biobased products from biorefinery carbohydrates—the US Department of Energy’s “Top 10” revisited. *Green Chemistry* **2010**, *12* (4), 539-554.

130. Kulkarni, R. K.; Moore, E. G.; Hegyeli, A. F.; Leonard, F., Biodegradable poly (lactic acid) polymers. *Journal of biomedical materials research* **1971**, *5* (3), 169-181.
131. Södergård, A.; Stolt, M., Properties of lactic acid based polymers and their correlation with composition. *Progress in polymer science* **2002**, *27* (6), 1123-1163.
132. Garlotta, D., A literature review of poly (lactic acid). *Journal of Polymers and the Environment* **2001**, *9* (2), 63-84.
133. Reddy, G.; Altaf, M. D.; Naveena, B. J.; Venkateshwar, M.; Kumar, E. V., Amylolytic bacterial lactic acid fermentation—a review. *Biotechnology advances* **2008**, *26* (1), 22-34.
134. Nwankwo, D.; Anadu, E.; Usoro, R., Cassava-fermenting organisms Microorganismes fermentant le manioc. *MIRCEN journal of applied microbiology and biotechnology* **1989**, *5* (2), 169-179.
135. Åkerberg, C.; Hofvendahl, K.; Zacchi, G.; Hahn-Hägerdal, B., Modelling the influence of pH, temperature, glucose and lactic acid concentrations on the kinetics of lactic acid production by *Lactococcus lactis* ssp. *lactis* ATCC 19435 in whole-wheat flour. *Applied microbiology and biotechnology* **1998**, *49* (6), 682-690.
136. Holm, M. S.; Saravanamurugan, S.; Taarning, E., Conversion of Sugars to Lactic Acid Derivatives Using Heterogeneous Zeotype Catalysts. *Science* **2010**, *328* (5978), 602.
137. Noike, T.; Takabatake, H.; Mizuno, O.; Ohba, M., Inhibition of hydrogen fermentation of organic wastes by lactic acid bacteria. *International journal of hydrogen energy* **2002**, *27* (11-12), 1367-1371.
138. Guo, Q.; Fan, F.; Pidko, E. A.; Van Der Graaff, W. N. P.; Feng, Z.; Li, C.; Hensen, E. J. M., Highly Active and Recyclable Sn-MWW Zeolite Catalyst for Sugar Conversion to Methyl Lactate and Lactic Acid. *ChemSusChem* **2013**, *6* (8), 1352-1356.
139. West, R. M.; Holm, M. S.; Saravanamurugan, S.; Xiong, J.; Beversdorf, Z.; Taarning, E.; Christensen, C. H., Zeolite H-USY for the production of lactic acid and methyl lactate from C3-sugars. *Journal of Catalysis* **2010**, *269* (1), 122-130.
140. de Clippel, F.; Dusselier, M.; Van Rompaey, R.; Vanelderen, P.; Dijkmans, J.; Makshina, E.; Giebler, L.; Oswald, S.; Baron, G. V.; Denayer, J. F. M., Fast and selective sugar conversion to alkyl lactate and lactic acid with bifunctional carbon–silica catalysts. *Journal of the American chemical society* **2012**, *134* (24), 10089-10101.
141. Taarning, E.; Osmundsen, C. M.; Yang, X.; Voss, B.; Andersen, S. I.; Christensen, C. H., Zeolite-catalyzed biomass conversion to fuels and chemicals. *Energy & Environmental Science* **2011**, *4* (3), 793-804.

142. Murillo, B.; Zornoza, B.; de la Iglesia, O.; Téllez, C.; Coronas, J., Chemocatalysis of sugars to produce lactic acid derivatives on zeolitic imidazolate frameworks. *Journal of Catalysis* **2016**, *334*, 60-67.
143. Pan, Y.; Liu, Y.; Zeng, G.; Zhao, L.; Lai, Z., Rapid synthesis of zeolitic imidazolate framework-8 (ZIF-8) nanocrystals in an aqueous system. *Chemical Communications* **2011**, *47* (7), 2071-2073.
144. Qian, J.; Sun, F.; Qin, L., Hydrothermal synthesis of zeolitic imidazolate framework-67 (ZIF-67) nanocrystals. *Materials Letters* **2012**, *82*, 220-223.

